Inorganic Chemistry

Article

pubs.acs.org/IC

Silylamide Complexes of Chromium(II), Manganese(II), and Cobalt(II) Bearing the Ligands $N(SiHMe_2)_2$ and $N(SiPhMe_2)_2$

Sonja N. König, Christoph Schädle, Cäcilia Maichle-Mössmer, and Reiner Anwander*

Institut für Anorganische Chemie, Universität Tübingen, Auf der Morgenstelle 18, 72076 Tübingen, Germany

Supporting Information

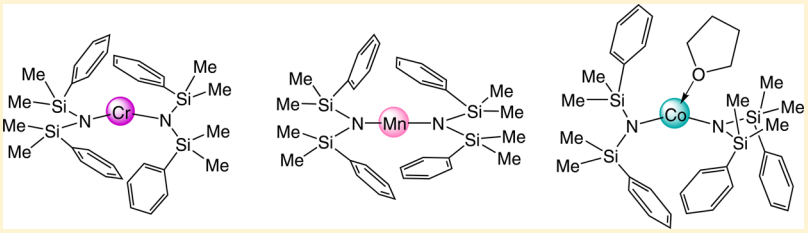

ABSTRACT: Bis(dimethylsilyl)amide and bis(dimethylphenylsilyl)amide complexes of the divalent transition metals chromium, manganese, and cobalt were synthesized. Dimeric, donor-free $\{Mn[N(SiHMe_2)_2]_2\}_2$ could be obtained via two different pathways, a salt metathesis route (utilizing $MnCl_2(thf)_{1.5}$ and $LiN(SiHMe_2)_2$) and a transsilylamination protocol (utilizing $Mn[N(SiMe_3)_2]_2(thf)$ and $HN(SiHMe_2)_2$). Addition of 1,1,3,3-tetramethylethylendiamine (tmeda) to $\{Mn[N(SiHMe_2)_2]_2\}_2$ yielded the monomeric adduct $Mn[N(SiHMe_2)_2]_2(tmeda)$. The syntheses of $Cr[N(SiHMe_2)_2]_2(tmeda)$, $Co[N(SiMe_3)_2][N(SiHMe_2)_2](tmeda)$, and $Co[N(SiHMe_2)_2]_2(tmeda)$ were achieved by transsilylamination from $Cr[N(SiMe_3)_2]_2(tmeda)$ and $\{Co[N(SiMe_3)_2]_2\}_2(\mu\text{-tmeda})$, respectively. Bis(dimethylphenylsilyl)amide complexes $Mn[N(SiMe_2Ph)_2]_2$, $Cr[N(SiMe_2Ph)_2]_2$, and $Co[N(SiMe_2Ph)_2]_2(thf)$ were obtained via salt metathesis employing $MCl_2(thf)_x$ (M = Cr, Mn, Co) with equimolar amounts of $LiN(SiMe_2Ph)_2$ in *n*-hexane. Treatment of $CrCl_2$ with $LiN(SiMe_2Ph)_2$ in thf gave $Cr[N(SiMe_2Ph)_2]_2(thf)_2$, featuring an almost square planar *trans*-coordination. All complexes were examined by elemental analyses, DRIFT and UV−vis spectroscopy, as well as X-ray structure analysis, paying particular attention to secondary M---SiH β-agostic and M---π(arene) interactions. Magnetic moments were determined by Evans' method.

INTRODUCTION

Silylamido ligands of type $-N(SiR_3)_2$ (R = any organic group) are known to ideally stabilize low coordination numbers of transition metal complexes; especially the archetypal bis(trimethylsilyl)amido ligand ($-N(SiMe_3)_2$) has been frequently used.[1] The respective complexes $M[N(SiMe_3)_2]_x$ (x = 1, 2, or 3) have been fully characterized for the 3d-transition metals except for nickel.[2] Furthermore, their syntheses are straightforward with moderate to high yields, and the resulting complexes are soluble in hydrocarbon solvents such as *n*-hexane. Crucially, complexes $M[N(SiMe_3)_2]_x$ qualify as precursors for other metallorganic species since protic exchange yields only the free silylamine as a side product ($pK_a[HN(SiMe_3)_2]$ = 25.8),[2,3] which can be removed very easily under vacuum. For example, clusters exhibiting magnetic properties can be synthesized from $Mn[N(SiMe_3)_2]_2$, $Fe[N(SiMe_3)_2]_2$, and $Co[N(SiMe_3)_2]_2$ by protic exchange of the silylamido ligand with 8-aminoquinoline or hexahydropyrimidopyrimidine.[4] Complexes $M[N(SiMe_3)_2]_2$ (M = Fe, Co) and their donor adducts were successfully employed as homogeneous catalysts, e.g., for the hydrosilylation of carbonyl compounds,[5] as well as to design single-molecule magnets.[6] Transition metal silylamide complexes have also been used as molecular precursors for metals, metal alloys, carbides, nitrides, oxides, and silicates according to chemical vapor deposition[2o,7] and ammonolysis techniques.[8] More recently, complexes $M[N(SiMe_3)_2]_2$, and in particular iron and cobalt derivatives, were comprehensively studied as precursors for magnetic nanoparticles.[9−11]

Our group has been investigating metal silylamides not only as synthesis precursors for homogeneous catalysts according to silylamine[12] and silylamide elimination protocols[13,14] but also as reactants for the surface functionalization of silica materials. Metal silylamides engage in efficient mild surface grafting if compared to metal alkyls and metal alkoxides, which tend to undergo multifunctional surface reactions and lead to incomplete consumption of the silanol groups, respectively.[15] Silylamide complexes employed so far for the functionalization of silica surfaces comprise the ligands $[N(SiMe_3)_2]$, $[N(SiHMe_2)_2]$, and $[N(SiMe_2Ph)_2]$.[15,16] For example, $Cr[N(SiMe_3)_2]_2(thf)_2$ can be immobilized on silica gel and applied in ethylene polymerization.[17] By grafting $Ca[N(SiMe_3)_2]_2$ onto Aerosil 380 silica, the mostly unwanted Schlenk equilibrium can be prevented (the latter occurs when aiming at heteroleptic complexes of the type $Ca[N(SiMe_3)_2][OSi(O^tBu)_3]$); moreover, these heterogenized "heteroleptic" catalysts show promising activity in the hydrosilylation of alkenes.[18] $Ln[N(SiMe_3)_2]_3$/SBA-15 hybrid materials (Ln = Y, La, Nd; SBA-15

Received: February 3, 2014
Published: April 24, 2014

 © 2014 American Chemical Society dx.doi.org/10.1021/ic5002682 | Inorg. Chem. 2014, 53, 4585−4597

Scheme 1. Synthesis Routes and Schematic Drawing of Compound 1

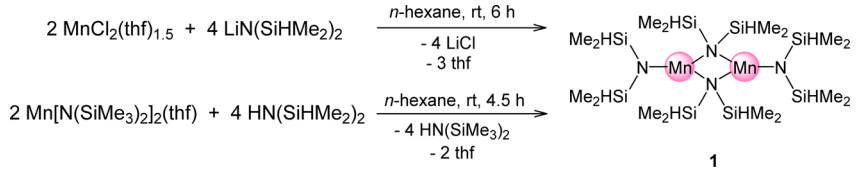

= high-surface periodic mesoporous silica) exhibit better performance than in the intramolecular hydroamination cyclization of aminoalkenes than the molecular counterparts.[19] Grafting of lanthanide and aluminum bis(dimethylsilyl)amide complexes $M[N(SiHMe_2)_2]_3(thf)_x$ and subsequent ligand exchange against 1,1,1,2,2,3,3-heptafluoro-7,7-dimethyl-4,6-octanedione generates surface species that are active in the hetero-Diels–Alder cyclization (Danishefsky transformation).[20] The surface chemistry of bis(dimethylphenylsilyl)amide complexes is less exploited. Only $Mg[N(SiMe_2Ph)_2]_2$ and $Fe[N(SiMe_2Ph)_2]_2$ have been grafted onto cage-like periodic mesoporous silica until now.[21]

The transsilylamination route offers a straightforward protocol for the synthesis of bis(dimethylsilyl)amide complexes ($pK_a[N(SiHMe_2)_2] = 22.8$).[22,23] Moreover, the ligand is an excellent IR/NMR spectroscopic probe,[15] allowing for an easy monitoring of ligand exchange and surface reactions. Bis(dimethylsilyl)amide complexes have been synthesized for most rare-earth metals[23−26] and alkaline-earth metals,[21b,27] as well as group 13 metals.[28] In contrast, only a few transition metal bis(dimethylsilyl)amide complexes have been described in the literature so far; namely, homoleptic $Hf[N(SiHMe_2)_2]_4$,[7e] $U[N(SiHMe_2)_2]_4$,[29] $\{Fe(II)[N(SiHMe_2)_2]_2\}_2$,[21a] and $Zn[N(SiHMe_2)_2]_2$[30] and heteroleptic $Mo_2(O_2CR)_2[N(SiHMe_2)_2]_2(PR'_3)_2$ (R = Me, ^{t}Bu; PR'_3 = PMe_3, PMe_2Ph, PEt_3),[31] $M[N(SiHMe_2)_2]_3(NSiHMe_2)$ (M = Nb, Ta),[32] $Zr[N(SiHMe_2)_2]_2Cl_2$,[33] $Ti[N(SiHMe_2)_2](NMe_2)_3$,[34] and $Fe(III)[N(SiHMe_2)_2]_3(\mu\text{-}Cl)Li(thf)_3$[21a] are known.

Exchanging the hydrogen atom in a Si–H group for a phenyl group leads to the similar ligand bis(dimethylphenyl)silylamide ($-N(SiMe_2Ph)_2$). This ligand is more bulky but able to establish π-interactions with the metal centers. Only five homoleptic metal amides with this ligand have been synthesized to date, $\{LiN(SiMe_2Ph)_2\}_2$,[35] $Fe[N(SiMe_2Ph)_2]_2$,[36] $\{Cu[N(SiMe_2Ph)_2]\}_4$,[37] $Cd[N(SiMe_2Ph)_2]_2$,[38] and $Sn[N(SiMe_2Ph)_2]_2$,[39] illustrating that this ligand can stabilize monomeric species of divalent metals.

In this work, we present the synthesis of Cr(II), Mn(II), and Co(II) bis(dimethylsilyl)amide and bis(dimethylphenylsilyl)amide complexes and their analytical characterization including X-ray structure analysis.

RESULTS AND DISCUSSION

Synthesis of Bis(dimethylsilyl)amide Complexes. Homoleptic manganese(II) bis(dimethylsilyl)amide **1** can be synthesized via a salt metathesis route from $MnCl_2(thf)_{1.5}$ or via transsilylamination from $Mn[N(SiMe_3)_2]_2(thf)$.[40] In both cases, crystallization from *n*-hexane affords the donor-free dimeric structure of $\{Mn[N(SiHMe_2)_2]_2\}_2$ (**1**, Scheme 1).

The molecular structure of **1** (Figure 1, Table 1, Table 5) is similar to those of $\{Mn[N(SiMe_3)_2]_2\}_2$[2k] and $\{Fe[N(SiHMe_2)_2]_2\}_2$,[21a] revealing a dimeric structure with two bridging and two terminal silylamido moieties, causing a distorted trigonal configuration of the metal centers. Compared

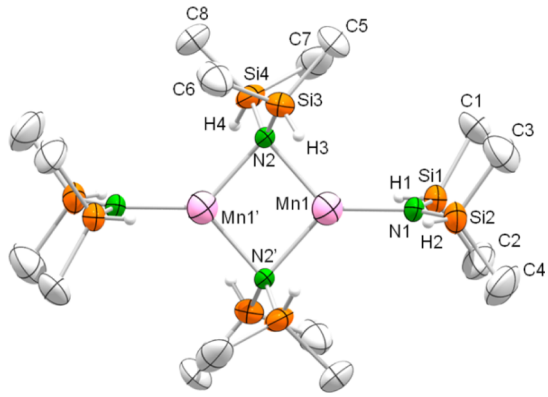

Figure 1. ORTEP view of complex **1**. The atomic displacement parameters are set at the 50% probability level; hydrogen atoms of the methyl groups are omitted for clarity.

Table 1. Selected Interatomic Distances and Angles of Compound 1 and $\{Fe[N(SiHMe_2)_2]_2\}_2$[21a]

	1	$\{Fe[N(SiHMe_2)_2]_2\}_2$
	Bond Lengths/Interatomic Distances(Å)	
M1–N1	1.984(4)	1.903(2)
M1–N2	2.129(4)	2.017(2)
M1–N2′	2.123(4)	2.050(2)
M1---M1′	2.849(2)	2.6733(6)
M1---Si1	2.994(2)	3.0821(8)
M1---Si2	3.218(2)	3.0794(7)
M1---Si3	3.000(2)	3.1324(7)
M1---Si4	3.354(3)	3.2573(7)
	Angles (deg)	
N1–M1–N2	132.4(2)	134.96(7)
M1–N2–M1′	84.2(1)	82.18(6)
N2–M1–N2′	95.9(1)	97.82(6)
Si1–N1–Si2	129.5(3)	126.49(1)
Si3–N2–Si4	123.2(2)	117.43(9)
Mn1–N1–Si1	109.1(3)	116.8(1)
Mn1–N1–Si2	121.4(3)	116.7(1)
Mn1–N2–Si3	101.7(2)	111.57(9)
Mn1–N2–Si4	120.1(3)	118.93(9)

to the corresponding bis(trimethylsilyl)amide complex of manganese(II) the terminal Mn–N distances are very similar (1.984 vs 1.994 Å)[2k] and the Mn–N distances to the bridging ligands are slightly shorter by ca. 0.06 Å (2.123 vs 2.184 Å),[2k] which apparently arises from the lower steric demand of the bis(dimethysilyl)amido ligand. This phenomenon has also been observed for the dimeric bis(dimethylsilyl)amide and bis(trimethylsilyl)amide complexes of iron(II).[21a] Furthermore, the Mn1–N2–Mn1′ angle of 84.2° is wider than in $\{Mn[N(SiMe_3)_2]_2\}_2$ (81.1°),[2k] giving an almost square planar core for complex **1**, while the distances between the manganese atoms Mn1---Mn1′ are almost the same in both complexes (Δd: 0.008 Å). The crystal structure of the iron(II)

dx.doi.org/10.1021/ic5002682 | Inorg. Chem. 2014, 53, 4585−4597

Table 2. Selected Interatomic Distances and Angles of Compounds 4, 5, 6, and 7

	4 (Cr)	7 (Mn)	5 (Co)	6 (Co)
		Bond Angles (deg)		
M1−N1	2.046(2)	2.0470(7)	1.9750(8)	1.968(1)
M1−N2	2.048(2)	2.0475(7)	1.9761(8)	1.975(1)
M1−N3	2.209(2)	2−2901(7)	2.2075(8)	2.184(1)
M1−N4	2.225(2)	2.3020(7)	2.1842(9)	2.184(1)
M1---Si1	3.1430(7)	3.2915(3)	3.2146(3)	3.0873(4)
M1---Si2	3.2197(7)	3.0930(3)	3.1284(3)	3.2196(5)
M1---Si3	3.1484(7)	3.2306(3)	3.1485(3)	3.2698(5)
M1---Si4	3.2759(7)	3.2345(3)	3.2043(3)	2.9382(4)
		Bond Lengths/Interatomic Distances (Å)		
N1−M1−N2	100.85(7)	124.57(3)	117.32(3)	116.33(5)
N1−M1−N3	91.25(7)	119.21(3)	101.92(3)	106.68(5)
N1−M1−N4	163.58(7)	102.09(3)	121.33(3)	121.19(5)
N2−M1−N3	163.78(7)	102.80(3)	124.27(3)	118.76(5)
N2−M1−N4	91.21(7)	120.13(3)	105.55(4)	106.69(5)
N3−M1−N4	79.29(7)	80.37(3)	82.93(3)	83.50(5)
M1−N1−Si1	114.19(8)	122.90(4)	121.73(5)	114.31(6)
M1−N1−Si2	118.72(8)	110.94(3)	116.31(4)	122.43(7)
M1−N2−Si3	114.35(8)	118.79(4)	116.89(4)	125.81(7)
M1−N2−Si4	121.81(9)	119.12(4)	120.87(5)	105.81(6)

Table 3. Selected Bond Lengths and Angles of Compounds 8, 9, 10, 11, and $Fe[N(SiMe_2Ph)_2]_2$[36]

	9 (Cr)	11 (Cr)	8 (Mn)	$Fe[N(SiMe_2Ph)_2]_2$[36]	10 (Co)
			Bond Lengths/Interatomic Distances (Å)		
M1−N1	2.0031(8)	2.078(1)	1.968(2)	1.896(2)	1.925(1)
M1−N2	1.9550(8)		1.976(2)	1.909(2)	1.922(1)
M1---C3	3.8699(9)	3.866(1)	3.046(2)	3.013(3)	4.388(1)
M1---C11	2.379(1)	4.622(1)	3.279(2)	3.227(3)	3.920(1)
M1---C19	3.191(1)		3.068(2)	2.956(3)	3.889(1)
M1---C27	3.113(1)		3.099(2)	3.234(4)	4.219(1)
M1−O1		2.1083(9)			2.0549(9)
			Bond Angles (deg)		
N1−M1−N2	140.89(4)	180.00	172.66(7)	172.1(1)	146.49(4)
M1−N1−Si1	133.19(5)	116.36(5)	115.47(9)	113.9(1)	110.15(5)
M1−N1−Si2	99.85(4)	118.35(5)	119.03(9)	119.5(1)	124.79(5)
M1−N2−Si3	116.29(4)		115.81(9)	113.2(1)	125.41(5)
M1−N2−Si4	115.89(5)		116.01(8)	119.1(1)	107.77(5)
N1−M1−O1		91.38(3)			104.68(4)
N2−M1−O1					108.83(4)
N1−M1−O1′		88.62(3)			

Table 4. Effective Magnetic Moments Determined by the Evans' Method

compound	μ_{eff} (μ_B)
$\{Mn[N(SiHMe_2)_2]_2\}_2$ (1)	3.26
$Cr[N(SiMe_3)_2]_2$(tmeda) (2)	4.82
$\{Co[N(SiMe_3)_2]_2\}_2$(μ-tmeda) (3)	5.09
$Cr[N(SiHMe_2)_2]_2$(tmeda) (4)	4.38
$Co[N(SiHMe_2)_2]_2$(tmeda) (6)	4.50
$Mn[N(SiHMe_2)_2]_2$(tmeda) (7)	5.97
$Mn[N(SiMe_2Ph)_2]_2$ (8)	5.74
$Cr[N(SiMe_2Ph)_2]_2$ (9)	4.69
$Co[N(SiMe_2Ph)_2]_2$(thf) (10)	5.20
$Cr[N(SiMe_2Ph)_2]_2(thf)_2$ (11)	4.54

bis[bis(dimethylsilyl)amide] exhibits shorter metal−nitrogen and metal---metal distances (Table 1), which probably arises from the smaller ionic radius of iron(II)[41] compared to manganese(II). In the manganese(II) complex (1), all Si−H protons are arranged in an eclipsed manner and face the metal center. In the case of $\{Fe[N(SiHMe_2)_2]_2\}_2$, the silicon groups of the bridging ligand are residing in a *gauche* conformation, meaning one Si−H proton is pointing away from the iron atom. Dimeric structures of bis(dimethylsilyl)amide complexes with two bridging bis(dimethylsilyl)amido ligands have also been observed for the trivalent rare-earth metals $\{Y[N(SiHMe_2)_2]_3\}_2$[24d] and $\{La[N(SiHMe_2)_2]_3\}_2$.[24g]

In the case of chromium(II) and cobalt(II), we were not able to access the donor-free bis(dimethylsilyl)amide complexes. Instead, degradation was observed during the attempted syntheses, via either salt metathesis or transsilylamination. Apparently, even the donor abilities of thf are too weak to stabilize this kind of compound. Adding the more powerful, potentially chelating donor tetramethylethylendiamine (tmeda) to $Cr[N(SiMe_3)_2]_2(thf)_2$[2g] and $Co[N(SiMe_3)_2]_2(thf)$[9a,42] gives $Cr[N(SiMe_3)_2]_2$(tmeda) (2) and $\{Co[N(SiMe_3)_2]_2\}_2$(μ-tmeda) (3, Scheme 2), respectively, which thereinafter enable

dx.doi.org/10.1021/ic5002682 | Inorg. Chem. 2014, 53, 4585−4597

Table 5. Crystallographic Data of Bis(dimethylsilyl)amide Complexes 1, 4, 5, 6, and 7

	1 (Mn)	4 (Cr)	5 (Co)	6 (Co)	7 (Mn)
fw (g/mol)	639.25	432.89	467.87	439.82	435.83
T (K)	293(2)	173(2)	100(2)	100(2)	103(2)
space group	triclinic $P\bar{1}$	monoclinic $P2_1/c$	monoclinic $P2_1$	monoclinic $P2_1/n$	monoclinic $P2_1/n$
a, b, c (Å)	7.975(3), 10.783(3), 11.595(3)	9.9205(8), 13.7329(8), 18.819(2)	9.3416(3), 17.7835(4), 10.2637(3)	10.0324(2), 17.8533(4), 14.3726(4)	11.0741(4), 15.4342(5), 14.9391(5)
α, β, γ (deg)	100.84(2), 106.62(2), 92.48(2)	94.381(7)	104.198(1)	95.706 (1)	96.043(2)
V (Å^3)	933.4(5)	2556.3(4)	1374.14(7)	2561.5(1)	2539.2(2)
Z	1	4	2	4	4
d_{calc} (g/cm^3)	1.137	1.125	1.131	1.140	1.140
R_1[a]	0.0777	0.0389	0.0171	0.0277	0.0195
wR_2[b]	0.2198	0.0967	0.0470	0.0707	0.0541
GOF[c]	1.085	1.153	1.033	1.020	1.061

[a] $R_1 = \sum(|F_o| - |F_c|)/\sum|F_o|$, $F_o > 2\sigma(F_o)$. [b] $wR_2 = \{\sum[w(F_o^2 - F_c^2)^2/\sum[w(F_o^2)^2]\}^{1/2}$. [c] GOF $= [\sum w(F_o^2 - F_c^2)^2/(n_0 - n_p)]^{1/2}$.

Scheme 2. Syntheses and Schematic Drawings of Compounds 2 and 3

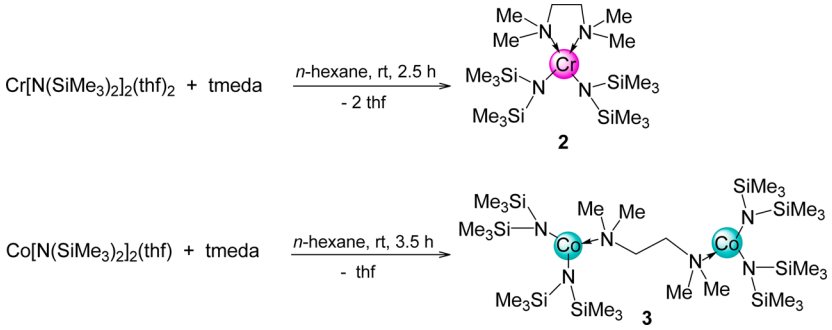

the syntheses of the bis(dimethylsilyl)amide complexes. Later on, the stabilizing effect of the newly introduced donor tmeda on the transsilylamination reactions to give the respective bis(dimethylsilyl)amido compounds was exploited in one-pot-reactions, without preceding isolation of the tmeda adducts **2** and **3**. Nevertheless, we were interested in the structural chemistry of both compounds. As illustrated in Scheme 2, the cobalt(II) complex **3** is binuclear with one bridging tmeda molecule and consequently three-coordinate for each cobalt atom, whereas the chromium(II) complex **2** is monomeric and four-coordinate. This finding probably arises from the different ionic radii of the two metals, with Cr(II) being the larger ion[41] and hence being able to coordinate both donor atoms of tmeda.

The DRIFT (diffuse reflectance infrared Fourier transform) spectra of **2** and **3** show only slight differences (Figure 2). The C−H valence vibration of the Si−CH_3 methyl groups (3030−2890 cm^{-1}), the C−H stretching vibration of the N−CH_3 methyl groups (2850−2800 cm^{-1}), the C−H bending vibration of the methylene and methyl groups (1480−1460 cm^{-1}), the C−N vibration at about 1250 cm^{-1}, and the Si−CH_3 valence vibration around 1240 cm^{-1} can be readily assigned. The asymmetric metal−nitrogen stretching vibrations are located at 377 (**2**) and 365 (**3**) cm^{-1} (Figures S1 and S2).

The molecular structure of **2** is depicted in Figure 3. Similar structures have been reported for calcium(II)[43] and ytterbium(II),[44] but in contrast to compound **2**, the latter display a center of symmetry (C_2 axis). Moreover, the angle between the N1−Cr1−N2 plane and the N3−Cr1−N4 plane is much smaller in the case of complex **2**, with 35.86(7)° compared to 53.66° and 54.5(4)° for the calcium(II) and ytterbium(II) compounds,

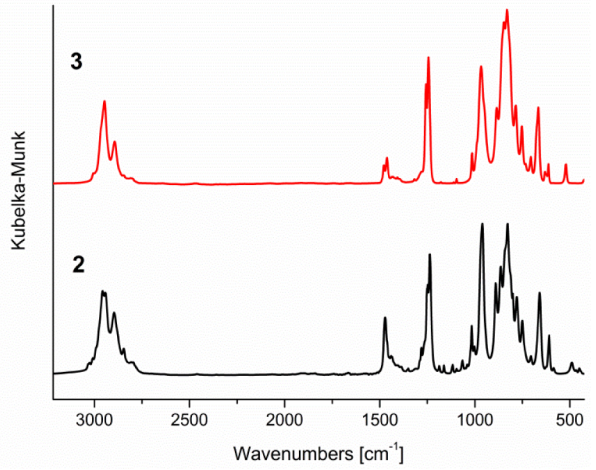

Figure 2. DRIFT spectra of compounds **2** and **3**.

respectively. Overall, in all three structures the metal centers adopt a distorted tetrahedral geometry. As expected, the M1−$N(SiMe_3)_2$ and M1−NMe_2 distances are somewhat longer for the previously described complexes (Yb(II): 2.34(1) and 2.61(1) Å; Ca: 2.315(1) and 2.592(2) Å).[43,44]

The core of {Co[$N(SiMe_3)_2$]$_2$}$_2$(μ-tmeda) (**3**, Figure 4) has an almost linear zigzag pattern propagating from N2 via the bridging tmeda to N3. The coordination geometry of the cobalt centers is distorted trigonal planar, and the M1−N bond lengths are shorter than in complex **2**. Other examples of tmeda bridging between two identical organometallic moieties have

dx.doi.org/10.1021/ic5002682 | Inorg. Chem. 2014, 53, 4585−4597

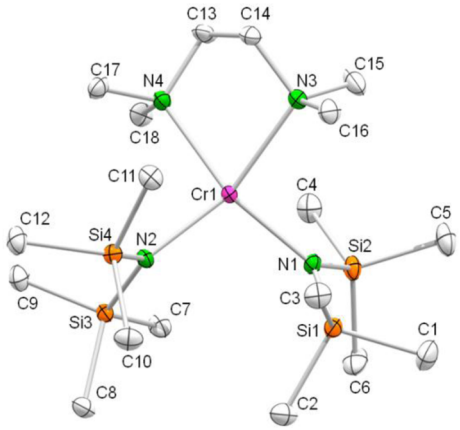

Figure 3. ORTEP view of complex **2** with the atomic displacement parameters set at the 50% probability level. Hydrogen atoms are omitted for clarity. Selected bond lengths (Å) and angles (deg): Cr1–N1 2.080(2), Cr1–N2 2.073(2), Cr1–N3 2.254(2), Cr1–N4 2.273(2), N1–Cr1–N2 106.76(8), N1–Cr1–N3 92.63(8), N1–Cr1–N4 152.01(8), N2–Cr1–N3 149.97(8), N2–Cr1–N4 92.40(8), N3–Cr1–N4 79.29(8).

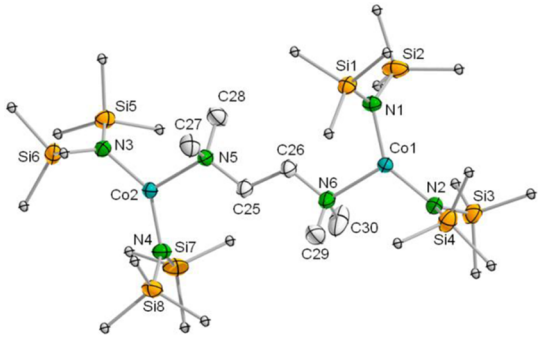

Figure 4. ORTEP view of complex **3** with the atomic displacement parameters set at the 50% probability level. Hydrogen atoms are omitted, and the methyl groups attached to silicon are shown in the ball and stick representation for clarity. Selected bond lengths/distances (Å) and angles (deg): Co1–N1 1.910(1), Co1–N2 1.915(1), Co1–N6 2.147(2), Co2–N3 1.910(1), Co2–N4 1.907(1), Co2–N5 2.151(1), Co1---Co2 7.3844(3), N1–Co1–N2 140.33(6), N1–Co1–N6 110.62(6), N2–Co1–N6 109.05(6), N3–Co2–N4 138.51(6), N3–Co2–N5 109.61(6), N4–Co2–N5 111.88(6).

been reported in the literature, for instance, $\{Co[N(Si^tBuMe_2)(2\text{-}C_5H_3N\text{-}6\text{-}Me)]_2\}_2(\mu\text{-tmeda})$,[45] $\{Co[PhC(NSiMe_3)(NAr)]_2\}_2(\mu\text{-tmeda})$ (Ar = 2,6-$Me_2C_6H_3$),[46] $[Al(SiMe_3)_3]_2(\mu\text{-tmeda})$,[47] or $[H_2GaN(SiHMe_2)]_2(\mu\text{-tmeda})$.[28c]

Applying tmeda as stabilizing donor, the transsilylamination protocol can be followed to generate the bis(dimethylsilyl)-amide complexes $Cr[N(SiHMe_2)_2]_2(tmeda)$ (**4**), $Co[N(SiMe_3)_2][N(SiHMe_2)_2](tmeda)$ (**5**), and $Co[N(SiHMe_2)_2]_2(tmeda)$ (**6**, Scheme 3). The reaction temperature of the transsilylamination of $\{Co[N(SiMe_3)_2]_2\}_2(\mu\text{-tmeda})$ with $HN(SiHMe_2)_2$ seems to be crucial, giving the mixed bis(trimethylsilyl)bis(dimethylsilyl)amide at ambient temperature (**5**) and the bis[bis(dimethylsilyl)amide)] at elevated temperatures (**6**). Since $-N(SiHMe_2)_2$ is sterically less demanding than $-N(SiMe_3)_2$, coordination of both donor atoms of tmeda to one cobalt center becomes feasible in **5** and **6**. For comparison only, the monomeric tmeda adduct of $\{Mn[N(SiHMe_2)_2]_2\}_2$ was synthesized by simply adding tmeda to a stirred solution of **1** in *n*-hexane. The only other known bis(dimethylsilyl)amide complex with additional tmeda coordination is the trivalent $La[N(SiHMe_2)_2]_3(tmeda)$.[48]

Comparing the angles between the planes spanned by the metal amido (N1–M1–N2) and the metal tmeda coordination (N3–M1–N4), complex **4** stands out with only 17.46(7)°, leading to a distorted square planar configuration of the chromium center. The interplanar angles for the cobalt (**5**, **6**) and manganese (**7**) are 74.38(3)°, 79.21(4)°, and 75.84(3)°, respectively, creating a distorted tetrahedral environment of the metal centers. The M1–N distances decrease with decreasing ionic radius of the metal (Mn1–N > Cr1–N > Co1–N). The terminal Mn1–N1 bond in **1** is shorter than the Mn1–N bonds in the tmeda adduct **7**, but the bridging Mn1–N2 and Mn1–N2′ bonds are slightly longer. The Si–H moieties in complexes **1** and **4**–**7** exhibit distinct orientations with respect to the metal centers. In some cases, somewhat shorter metal–silicon distances can be noticed, which is also reflected in slightly smaller M–N–Si angles. This is the case for Mn1---Si1 and Mn1---Si3 in **1**, Co1---Si4 in **6**, and Mn1---Si1 in **7** (Table 1, Table 2). These observations can denote weak *β*-agostic interactions between some of the Si–H bonds and the respective metal centers. Bis(trimethylsilyl)amide complexes of Mn(II) and Co(II) with additional coordination of 2,2′-bipyridyl (2,2′-bipy)[49] or two donor molecules such as pyridine (py),[50] pyrazine (prz),[50] and thf[51] are known in the literature. Similar to complexes **2** and **4**–**7**, the N–M–N angles spanned by the silylamido ligands are wider than the D–M–D angles spanned by the donor molecules (M = Mn, do = 2,2′-bipy: 128.24(17)° vs 72.91(18)°,[49] M = Mn, do = py: 127.18(3)° vs 86.77(3)°,[50] M = Co, do = py: 123.17(4)° vs 90.1(4)°,[50] M = Mn, do = prz: 130.82(7)° vs 96.23(7),[50] and M = Mn, do = thf: 131.7(2)° vs 86.6°[51]).

Scheme 3. Syntheses of Compounds 4, 5, 6, and 7 via a One-Pot tmeda Addition/Transsilylamination

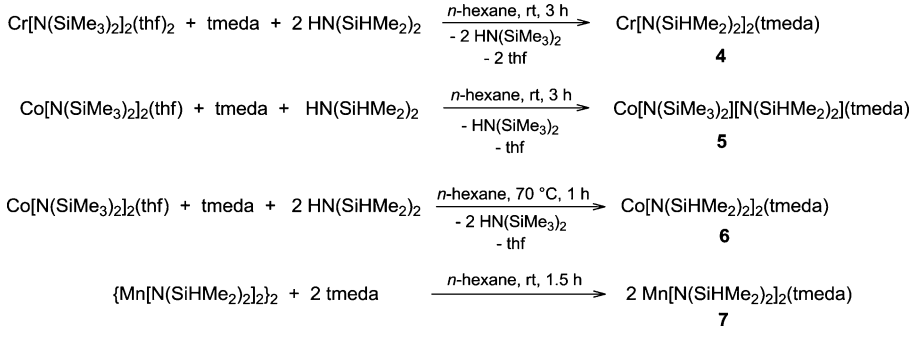

dx.doi.org/10.1021/ic5002682 | Inorg. Chem. 2014, 53, 4585–4597

The most prominent difference between the DRIFT spectra of **1**, **4**, **5**, **6**, and **7** (Figure 9) and the bis(trimethylsilyl)amide

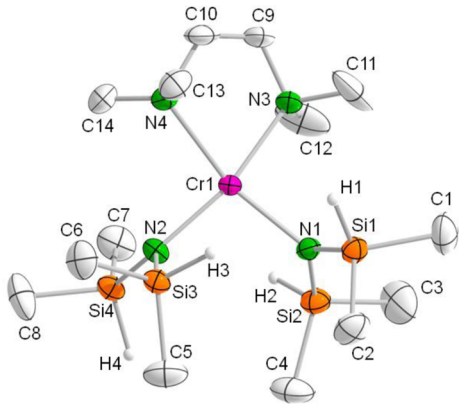

Figure 5. ORTEP view of complex **4** with the atomic displacement parameters set at the 50% probability level. C−H protons and the disorder of C9, C10, C13, and C14 are omitted for clarity.

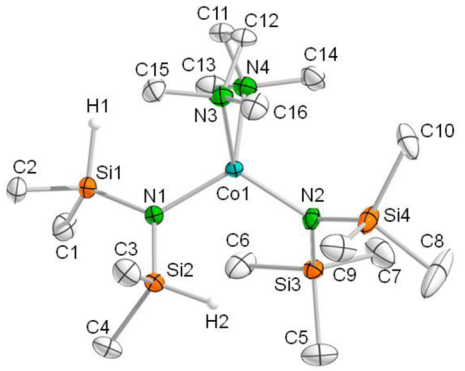

Figure 6. ORTEP view of complex **5** with the atomic displacement parameters set at the 50% probability level. C−H protons are omitted for clarity.

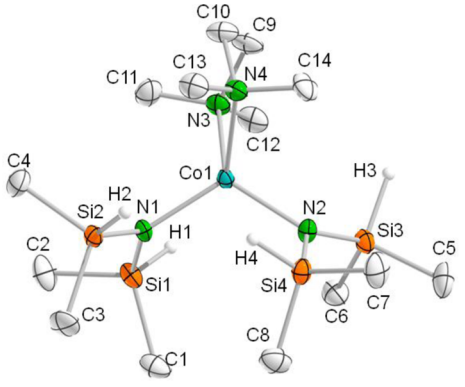

Figure 7. ORTEP view of complex **6** with the atomic displacement parameters set at the 50% probability level. C−H protons are omitted for clarity.

complexes **2** and **3** (Figure 2) is the Si−H valence vibration appearing in the region from 2130 to 2020 cm^{-1}. The Si−H deformation vibration can be found in the fingerprint region between 1010 and 700 cm^{-1}. The assignment of the remaining characteristic bands is equivalent to **2** and **3**. Infrared spectroscopy is a valuable tool to determine β-agostic interactions, since the heteroatom−hydrogen bond gets

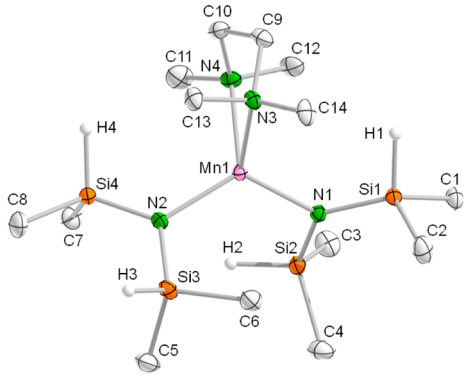

Figure 8. ORTEP view of complex **7** with the atomic displacement parameters set at the 50% probability level. C−H protons are omitted for clarity.

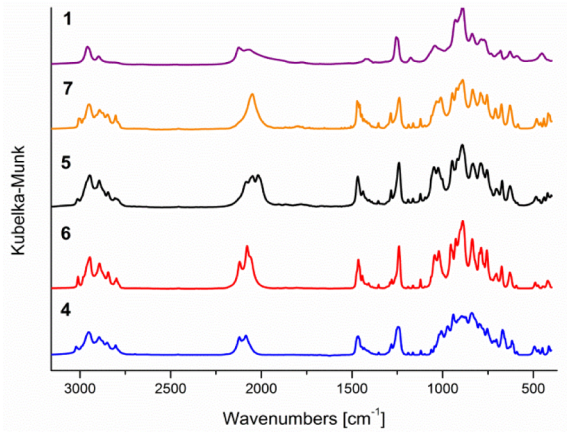

Figure 9. DRIFT spectra of compounds $\{Mn[N(SiHMe_2)_2]_2\}_2$ (**1**), $Mn[N(SiHMe_2)_2]_2(tmeda)$ (**7**), $Cr[N(SiHMe_2)_2]_2(tmeda)$ (**4**), $Co[N(SiMe_3)_2][N(SiHMe_2)_2](tmeda)$ (**5**), and $Co[N(SiHMe_2)_2]_2(tmeda)$ (**6**).

weakened and therefore the stretching mode is shifted to smaller wavenumbers.[33,52] For lanthanide and alkaline-earth metal bis(dimethylsilyl)amide complexes it has been found that the Si−H valence vibration can be shifted to values below 2000 cm^{-1} in the presence of significant β-agostic interactions.[23,25b,48] Such low-energy Si−H valence vibrations were not observed for the bis(dimethylsilyl)amide complexes **1**, **4**, **5**, **6**, and **7** (all bands lie above 2020 cm^{-1}), but the bands appear well resolved, e.g., revealing three distinct stretching modes for complex **5**. The discrepancy in the arrangement of the Si−H moieties that is observed in the solid-state structures is most likely caused by different effects including crystal packing. The asymmetric metal−nitrogen stretching vibrations of the monomeric tmeda adducts are located below 400 wavenumbers (Figures S3−S5) with 380 cm^{-1} for **4**, 351 cm^{-1} for **6**, and 343 cm^{-1} for **7**. In contrast, the asymmetric Mn−N stretching vibration in **1** can be found at 450 cm^{-1} (Figure S6).

Syntheses of Bis(dimethylphenylsilyl)amide Complexes. The reaction of $MnCl_2(thf)_{1.5}$ and $CoCl_2(thf)_{1.25}$ with 2 equiv of $LiN(SiMe_2Ph)_2$ in *n*-hexane gave donor-free $Mn[N(SiMe_2Ph)_2]_2$ (**8**) and donor-coordinated $Co[N(SiMe_2Ph)_2]_2(thf)$ (**10**), respectively. Applying the same method for $CrCl_2(thf)_x$ yielded the donor-free complex $Cr[N(SiMe_2Ph)_2]_2$ (**9**) and a minor amount of $Cr[N(SiMe_2Ph)_2]_2(thf)_2$ (**11**). The two compounds could be

dx.doi.org/10.1021/ic5002682 | Inorg. Chem. 2014, 53, 4585−4597

separated by fractional crystallization from *n*-hexane, giving first purple crystals of the donor adduct and then pale green crystals of the donor-free product. The former (**11**) can also be synthesized directly from $CrCl_2$ and 2 equiv of $LiN(SiMe_2Ph)_2$ in thf. The syntheses are straightforward (Scheme 4) and give the desired complexes in moderate yields.

Scheme 4. Syntheses of Compounds 8 to 11 via Salt Metathesis

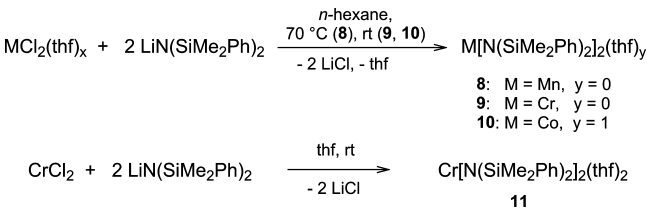

With manganese(II) being the largest of the three ions,[41] all four phenyl rings can be arranged around the metal center to saturate the coordination sphere (**8**, Chart 1). Chromium(II) is

Chart 1. Schematic Drawings of Compounds 8, 9, 10, and 11

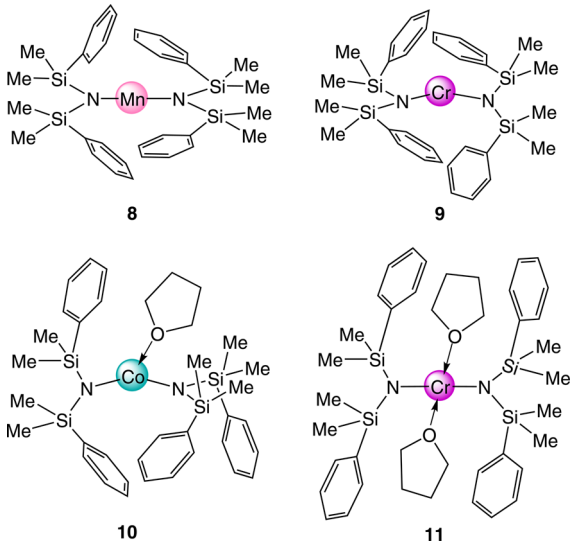

the second largest metal ion;[41] here only three phenyl rings face the metal center, while the fourth phenyl ring points in the opposite direction (**9**). Cobalt(II) is the smallest of the metal ions, and the phenyl rings exhibit rather large distances to the metal center (**10**). In this case, one thf molecule is needed to saturate the coordination sphere of a monomeric species. In contrast, the donor-coordinated Cr(II) complex (**11**) contains two thf molecules, probably because the bigger ionic radius requires one more thf to saturate the coordination sphere.

The fingerprint regions of the recorded DRIFT spectra of compounds **8** to **11** differ greatly, presumably depending on the interactions of the phenyl rings with the metal center and thf coordination (Figure 10). The characteristic peaks, being the C−H valence vibration of the aromatic rings and the methyl groups (3130−2995 and 2953−2894 cm^{-1}, respectively), the C−H bending vibration at around 1425 cm^{-1}, the Si−CH_3 valence vibration at 1245 cm^{-1}, and the aromatic C−H bending vibration at 1109 cm^{-1}, can be assigned (Figure S7). The bands of the asymmetric metal−nitrogen stretching vibration are similar for complexes **8**−**10**, at 382, 390, and 386 cm^{-1},

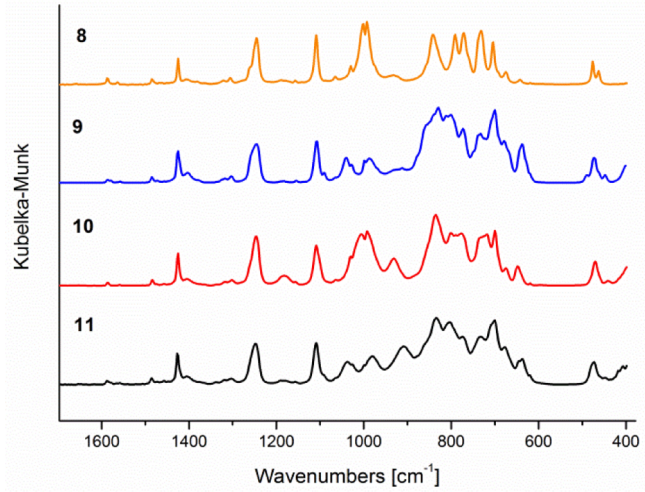

Figure 10. DRIFT spectra of compounds **8**, **9**, **10**, and **11** in the range from 1600 to 400 cm^{-1}.

respectively (Figures S8−S10). The asymmetric Cr−N stretching vibration in square planar complex **11** is located at 413 cm^{-1} (Figure S11).

The molecular structure of $Mn[N(SiMe_2Ph)_2]_2$ (**8**) is depicted in Figure 11. The N1−Mn1−N2 angle is almost

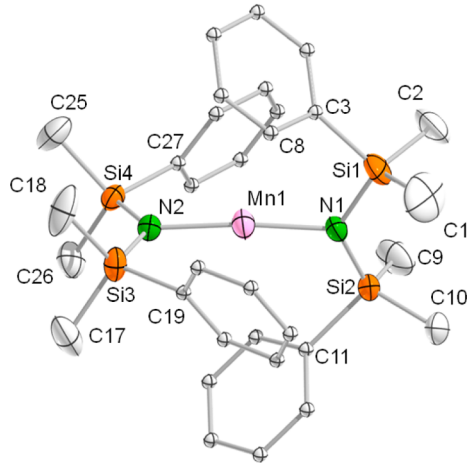

Figure 11. ORTEP view of molecule 1 of compound **8**. The atomic displacement parameters are set at the 50% probability level, hydrogen atoms are omitted for clarity, and the carbon atoms of the phenyl rings are shown in the ball and stick representation for clarity.

linear at 172.66(7)° and is very similar to the angle of the equivalent iron(II) complex $Fe[N(SiMe_2Ph)_2]_2$[36] (see Table 3). Bending of the L−M−L moiety has been observed for most two-coordinate open-shell transition metal complexes and can be due to intramolecular interactions between the metal center and the ligand backbone, packing forces, ligand field or hybridization effects, and Renner−Teller distortions.[53]

The Mn−N bonds in **8** are slightly longer in the corresponding iron compound, which is caused by the larger ionic radius of manganese(II) compared to iron(II).[41] The corresponding manganese(II) bis(diphenylmethylsilyl)amide $Mn[N(SiMePh_2)_2]_2$ exhibits longer Mn1−N distances (1.989(3) and 1.988(3) Å).[36] The same trend is observed for the Fe−N bond lengths in the iron(II) complexes $Fe[N(SiMe_2Ph)_2]_2$ and $Fe[N(SiMePh_2)_2]_2$, and the authors state

dx.doi.org/10.1021/ic5002682 | Inorg. Chem. 2014, 53, 4585−4597

that this arises from the sterically more demanding ligand possessing two phenyl groups.[36] The Si−N−Si angles of **8** are a bit smaller than in $Mn[N(SiMePh_2)_2]_2$ (125.4(1)° and 128.08(9)° vs 127.7(2)° and 131.8(2)°, respectively), which is probably also due to the less bulky ligand. The distances from the manganese center in **8** to the *ipso* carbon atoms of the phenyl rings are only differing by 0.397 Å, with an average value of d_{av} = 3.123 Å. For one of the phenyl rings, the *ipso* carbon (C3) does not show the shortest distance to the metal center, but the carbon atom in *ortho* position (C8) does (3.046(2) and 2.945(3) Å, respectively). Although the distances of the phenyl rings to the metal center are rather large, the arrangement of the ligands suggests secondary interactions. A pseudo-octahedral configuration geometry has also been reported for the respective iron(II) complex.[36]

The bending of N1−M−N2 in $Cr[N(SiMe_2Ph)_2]_2$ (**9**, 140.89(4)°) is stronger than in $Mn[N(SiMe_2Ph)_2]_2$ (**8**, 172.66(7)°) and $Fe[N(SiMe_2Ph)_2]_2$ (172.1(1)°)[36] but far less pronounced compared to other two-coordinate Cr(II) amides with bent structures, e.g., $Cr[N(H)Ar^{Me_6}]_2$ (120.9(5)°)[53] or $Cr[N(Ph)BMes_2]_2$ (Mes = 2,4,6-trimethylphenyl, 110.8(1)°)[54] (Table 3, Figure 12).[55] Only three phenyl rings are directed

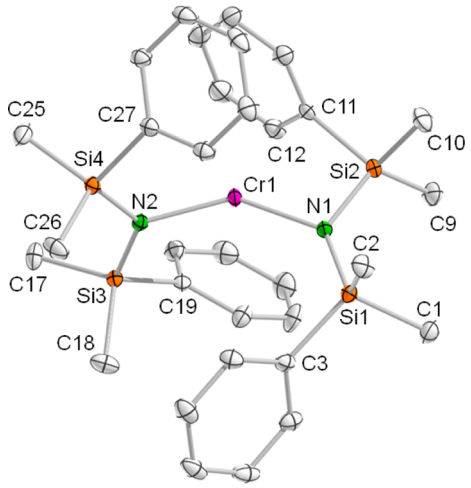

Figure 12. ORTEP view of complex **9**. The atomic displacement parameters are set at the 50% probability level; hydrogen atoms are omitted for clarity.

toward the chromium center in **9**. Furthermore, this complex exhibits larger variations in the Cr---C_{ipso} distances and the Cr1−N−Si angles (cf. Table 3). The Cr1−N1−Si1 angle is the widest and comes with the longest Cr1---C3 contact. Likewise, the shortest Cr---C_{ipso} distance corresponds to the smallest angle (Cr---C11 and Cr1−N1−Si2, cf. Table 3). In the latter case, the carbon atom in *ortho* position (C12) also exhibits a short contact to the chromium center (C11: 2.379(1) Å and C12: 2.524(1) Å). The distances are in the range of reported secondary interactions of phenyl rings with the metal center in two-coordinate arylamide complexes of divalent chromium, manganese, iron, cobalt, and nickel.[53,55−58] Short contacts to the *ipso* as well as the *ortho* carbon atom of phenyl rings in γ-position to the metal center have been reported for $\{Mn[CH_2CMe_2Ph]_2\}_2$[59] and tricarbonyl{2-[(1,2-η^2),κC^{α}-2-(phenylmethoxymethylene)phenyl]pyridine-κN}manganese-(I)[60] with distances of 2.728 and 2.639 Å or 2.240 and 2.438 Å, respectively.[59,60] From this it can be concluded that C11 and C12 seem to additionally coordinate to the chromium center in **9** in an η^2-coordination mode.

The N1−Co1−N2 angle of the cobalt complex $Co[N(SiMe_2Ph)_2]_2(thf)$ (**10**) is very similar to the angle of the chromium complex **9** (Figure 13, Table 3), but here an

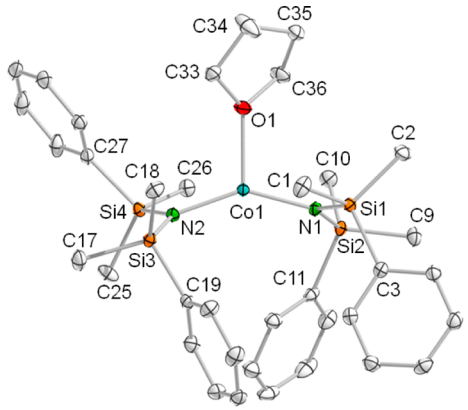

Figure 13. ORTEP view of complex **10**. The atomic displacement parameters are set at the 50% probability level; hydrogen atoms and disorder of C35 are omitted for clarity.

additional thf molecule is coordinated to the metal center. For $Co[N(SiMePh_2)_2]_2$, Chen et al.[36] state that the d^7 Co(II) ion prefers a pseudotetrahedral geometry, and thus the angle is bent. The Co1−N bonds of complex **10** are longer than in the equivalent bis(diphenylmethylsilyl)amide complex (1.898(3) and 1.904(3) Å, respectively), which is the reverse of what was observed for the manganese(II) and iron(II) complexes.[36] Most probably the additional coordination of thf gives rise to this bond elongation. The Co1---C_{ipso} distances in **10** are longer than in **8** and **9** (Table 3). Three-coordinate cobalt(II) centers in silylamide complexes have already been observed for $Co[N(SiMe_3)_2]_2(do)$ (do = thf,[9a,42] py,[50] or PPh_3[61]), and the N−Co−N angles in these compounds are even narrower than in **10** (141.80(16)°/141.89(9)°,[9a,42] 140.7(2)°,[50] and 130.7(7)°,[61] respectively). While the Co−N bonds in the phosphane-coordinated complex are similar to **10** (1.93(1) and 1.92(1) Å),[61] $Co[N(SiMe_3)_2]_2(thf)$ and $Co[N(SiMe_3)_2]_2(py)$ exhibit slightly shorter Co−N bond lengths (1.898(2)/1.9000(15)[9a,42] and 1.904(3) Å,[50] respectively).

Owing to the coordination of two thf molecules, the molecular structure of $Cr[N(SiMe_2Ph)_2]_2(thf)_2$ (**11**, Figure 14) is completely different from the aforementioned compounds (**8**, **9**, and **10**). Through the coordination of two thf molecules, an almost square planar coordination geometry of the chromium center is achieved, similarly to the bis(trimethylsilyl)amide complex $Cr[N(SiMe_3)_2]_2(thf)_2$[2g] (cf., Table 3). Moreover, the chromium atom depicts a center of symmetry as an inversion center. Compared to its donor-free homologue **9**, the Cr1−N1 bonds are longer, most likely originating from the additional coordination of thf.

Electronic Spectra. The UV−vis spectra of the manganese(II) compounds in *n*-hexane solution (**1**, **7**, and **8**) are essentially featureless, which is in accordance with their pale colors. The chromium(II) complexes (**2**, **4**, **9**, and **11**) mainly exhibit two bands in the UV−vis spectra, one in the range of 260−330 nm and the second above 620 nm (see Figures S12−S15). Two bands have as well been observed for other Cr(II) compounds, for example, $Cr[N(H)Ar^X]_2$ (X = Me_6, $^iPr_4$, $^iPr_6$)

dx.doi.org/10.1021/ic5002682 | Inorg. Chem. 2014, 53, 4585−4597

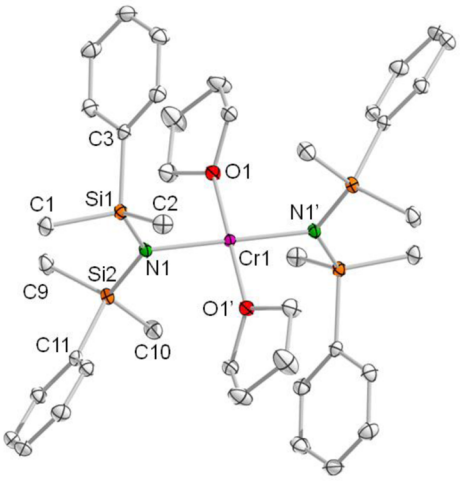

Figure 14. ORTEP view of complex **11**. The atomic displacement parameters are set at the 50% probability level; hydrogen atoms are omitted for clarity.

or $Cr[N(Ar)BMes_2]_2$ (Ar = Ph, Mes), but positioned in different ranges (333−345 and 400−417 nm for the former; 672/624 and 800 nm for the latter).[53,54] In the case of bis(dimethylphenylsilyl)amide complexes **9** and **11**, the $\pi\rightarrow\pi^*$ transition of the phenyl rings at around 261 nm can be additionally assigned (Figure S16). The UV−vis spectrum of cobalt complex $Co[N(SiMe_3)_2]_2(\mu\text{-tmeda})$ (**3**) with three-coordinate cobalt centers features four bands at 330, 414, 600, and 666 nm (Figure S17), which is very similar to $Co[N(SiMe_3)_2]_2(py)$ (318, 383, 647, 696 nm).[50] The UV−vis spectrum of dimeric $\{Co[N(SiMe_3)_2]_2\}_2$ in the liquid phase also showed four bands at accordant wavelengths (319, 410, 588, 680 nm).[2m] In *n*-hexane solution, however, the maxima are shifted to higher wavelengths (410, 585, 685, 1538 nm).[2m] The bis(dimethylsilyl)amide complex $Co[HN(SiHMe_2)_2]_2$(tmeda) (**6**) exhibits five bands (225, 316, 473, 632, 710 nm; Figure S18); unlike $Co[N(SiMe_3)_2]_2(py)_2$, which gave only three bands.[50] The last four bands in the UV−vis spectrum of **6** are positioned in similar ranges to those for **3** and $Co[N(SiMe_3)_2]_2$(py) (*vide supra*). For $Co[N(SiMe_2Ph)_2]_2$(thf) (**10**, Figure S19), the $\pi\rightarrow\pi^*$ transition of the phenyl rings can be found at 263 nm. Further bands are located at 360, 520, 629, and 791 nm, which is close to what was observed for corresponding $Co[N(SiMePh_2)_2]_2$ (526, 634, 802 nm).[36]

Magnetic Studies. Investigation of the magnetic moments has been carried out by Evans' method[62] in benzene/deuterated benzene and hexamethyldisiloxane as reference. In general, the determined μ_B-values are in accordance with d^4, d^5, and d^7 high-spin configurations (Table 4). Monomeric $Mn[N(SiHMe_2)_2]_2$(tmeda) (**7**) exhibits a magnetic moment of μ_{eff} = 5.97 μ_B, which is almost identical with the spin-only value for a d^5 high-spin electron configuration (5.92 μ_B). In contrast, the donor-free manganese complex $\{Mn[N(SiHMe_2)_2]_2\}$ (**1**) shows an effective magnetic moment of only 3.26 μ_B. This low value suggests antiferromagnetic coupling of the two metal centers probably via the bridging nitrogen atoms, proving that the dimeric structure is retained in solution. This phenomenon has also been observed for $\{Mn[N(SiMe_3)_2]_2\}_2$ with a μ_B-value of 3.34.[2k] Furthermore, the analogous $\{Fe[N(SiHMe_2)_2]_2\}_2$ complex has been proven to be dimeric in solution, as well.[21a] For $Cr[N(SiHMe_2)_2]_2$(tmeda) (**4**) and $Co[N(SiHMe_2)_2]_2$(tmeda) (**6**), magnetic moments of 4.38 and 4.50 μ_B can be observed, which lie below the spin-only value in the case of chromium(II) (4.90 μ_B) and above the spin-only value for cobalt(II) (3.87 μ_B). These observations have also been made in the literature for Cr(II) and Co(II) complexes and have been ascribed to spin−orbit coupling.[50,55,58] The bis(trimethylsilyl)amide complex of chromium(II), $Cr[N(SiMe_3)_2]_2$(tmeda) (**2**), shows a magnetic moment of 4.82 μ_B, which is much closer to the spin-only value than in the bis(dimethylsilyl)amide complex **4** (*vide supra*). Square planar, thf-coordinated $Cr[N(SiMe_3)_2]_2(thf)_2$ exhibits a slightly higher magnetic moment of 4.93 μ_B.[2g] In contrast, the μ_B-value of also square planar $Cr[N(SiMe_2Ph)_2]_2(thf)_2$ (**11**) is significantly lower (4.54 μ_B). Compared to the donor-coordinated version, the magnetic moment in $Cr[N(SiMe_2Ph)_2]_2$ (**9**) is slightly higher (4.69 μ_B). Again, μ_B-values below the spin-only value have been observed in the literature for two-coordinate, bent chromium(II) complexes, due to spin−orbit coupling.[53,55] The magnetic moment of the analogous manganese(II) complex $Mn[N(SiMe_2Ph)_2]_2$ (**8**) was determined to be 5.74 μ_B, which is lower than in complex **7** and than the spin-only value (*vide supra*). Similar magnetic moments have been observed for corresponding $Mn[N(SiMePh_2)_2]_2$ (5.72 μ_B)[36] and $Mn[N(H)Ar^{\#}]_2$ (5.73 μ_B, $Ar^{\#}$ = C_6H_3-2,6-(C_6H_2-2,4,6-Me_3)$_2$).[57] The dinuclear cobalt(II) complex $\{Co[N(SiMe_3)_2]_2\}_2(\mu\text{-tmeda})$ (**3**), with three-coordinate cobalt centers, exhibits a magnetic moment of μ_{eff} = 5.09 μ_B (for the calculation of μ_{eff}, the molecular weight was divided by 2). A similar μ_B-value can be found for $Co[N(SiMe_2Ph)_2]_2(thf)$ (**10**) (5.20 μ_B), where the metal centers are also three-coordinate. Both are significantly higher than for complex **6**, with a four-coordinate cobalt center (*vide infra*). The bis(trimethylsilyl)amide complex of cobalt(II) with additional coordination of triphenylphosphane features a lower magnetic moment of 4.84 μ_B.[61] In contrast, magnetic moments of 5.883(3) and 5.269(5) μ_B for $Co[N(SiMe_3)_2]_2(thf)$ and $Co[N(SiMe_3)_2]_2(py)$, respectively, were determined by SQUID (superconduction quantum interference device) measurements.[42] The bis(diphenylmethylsilyl)amide complex $Co[N(SiMePh_2)_2]_2$ exhibits a relatively small μ_B-value of 4.42 μ_B.[36]

Conclusion. Bis(dimethylsilyl)amide and bis(dimethylphenylsilyl)amide complexes of chromium(II), manganese(II), and cobalt(II) were synthesized in moderate to high yields. In the case of the bis(dimethylsilyl)amide derivatives, a salt metathesis protocol (utilizing chloride precursors) was successful only for the synthesis of donor-free $\{Mn[N(SiHMe_2)_2]_2\}_2$. For chromium(II) and cobalt(II), transsilylamination (utilizing bis(trimethylsilyl)amide precursors in *n*-hexane) is a viable protocol, requiring, however, the presence of a (stabilizing) chelating donor such as tmeda. For the smallest metal center Co(II) complete transilylamination and formation of $Co[N(SiHMe_2)_2]_2$(tmeda) were observed only at elevated reaction temperatures. The IR spectra of the bis(dimethylsilyl)amide complexes under study feature characteristic SiH stretch vibration patterns in the nonagostic range. Monometallic bis(dimethylphenylsilyl)amide complexes $M(II)[N(SiMe_2Ph)_2]_2(thf)_x$ (M = Cr, x = 0, 2; M = Mn, x = 0; M = Co, x = 1) are straightforwardly accessible from chloride and lithium silylamide precursors. Depending on the metal size and the presence of donor solvent, secondary M---π(arene) interactions cause distinct coordination environments.

dx.doi.org/10.1021/ic5002682 | *Inorg. Chem.* 2014, 53, 4585−4597

EXPERIMENTAL SECTION

General Considerations. All reactions were carried out under a dry argon atmosphere using standard Schlenk or glovebox techniques (MBraun, MB250B, < 0.1 ppm of H_2O, O_2). The solvents were dried over Grubbs columns (MBraun, Solvent Purification System) and stored inside the glovebox. Elemental analyses were carried out on an Elementar Vario MICRO instrument. DRIFT spectra were measured on a Thermo Scientific Nicolet 6700 FTIR spectrometer using KBr powder and a DRIFT cell equipped with KBr windows. The spectra were recorded with 256 scans from 4000 to 400 cm^{-1} with a resolution of 2 cm^{-1}. FIR spectra were collected with a Vertex 70 spectrometer from PerkinElmer using Nujol mulls and CsI plates. The spectra were recorded from 680 to 200 cm^{-1} with 256 scans and a resolution of 2 cm^{-1}. UV−vis spectra of *n*-hexane solutions of the compounds have been measured with a Lambda 35 spectrophotometer from PerkinElmer. The spectra were collected from 1000 to 200 nm with a scan speed of 480 nm/min. The Evans' method[62] has been carried out on a Bruker AVII+500 at 298 K in benzene/deuterated benzene with hexamethyldisiloxane as reference. Concentrations of the complexes in benzene solution ranged from 6 to 9 mg/mL. Manganese(II) chloride (97%), cobalt(II) chloride (99%), chromium(II) chloride (97%), chromium(III) chloride (99.9%), 1,1,3,3-tetramethyldisilazane (97%), and 1,1,1,3,3,3-hexamethyldisilazane (98%) were purchased from ABCR. Sodium amide (95%), potassium bis(trimethylsilyl)amide (sublimed at 130 °C under HV prior to use), *n*-butyllithum (2.5 M in *n*-hexane), and tetramethylethylendiiamine (99.5%) were obtained from Sigma-Aldrich. 1,3-Diphenyl-1,1,3,3-tetramethyldisilazane (96%) was acquired from Fluka. $LiN(SiHMe_2)_2$,[63] $LiN(SiMe_2Ph)_2$,[35,36] $NaN(SiMe_3)_2$,[64] $Mn[N(SiMe_3)_2]_2(thf)$,[65] $Cr[N(SiMe_3)_2]_2(thf)_2$,[2g] and $Co[N(SiMe_3)_2]_2(thf)$[9a,42] were synthesized according to literature procedures. Activated manganese(II) chloride and cobalt(II) chloride were generated by stirring the corresponding metal chloride in thf at ambient temperature; the thf content was calculated from elemental analyses.[66]

Synthesis of $\{Mn[N(SiHMe_2)_2]_2\}_2$ ***(1)***. Pathway A: $MnCl_2(thf)_{1.5}$ (184 mg, 0.77 mmol) was suspended in *n*-hexane, and $LiN(SiHMe_2)_2$ (216 mg, 1.55 mmol) in *n*-hexane was added. The mixture turned pink gradually. After stirring for 6 h at ambient temperature, LiCl was separated by centrifugation. The combined *n*-hexane fractions were dried under vacuum, yielding a rose solid. Crystallization from *n*-hexane gave rose crystals. Yield: 198 mg, 80%. Pathway B: $Mn[N(SiMe_3)_2]_2(thf)$ (102 mg, 0.23 mmol) was dissolved in *n*-hexane, and $HN(SiHMe_2)_2$ (67 mg, 0.50 mmol) was added. The pink solution was stirred for 4.5 h at ambient temperature, and then the solvent was removed under vacuum. Crystallization from *n*-hexane yielded rose crystals. Yield: 51 mg, 70%. Anal. Calcd for $C_{16}H_{56}N_4Si_8Mn_2$: C 30.06, H 8.83, N 8.77. Found: C 29.98, H 9.03, N 8.61. DRIFT (KBr, cm^{-1}): 2959 (m), 2897 (w), 2125 (m), 2086 (b), 1174 (w), 1414 (w), 1255 (m), 1176 (w), 1043 (m), 930 (s), 890 (s), 837 (m), 785 (m), 770 (m), 733 (w), 680 (w), 628 (w), 591 (w), 454 (w). IR (Nujol, cm^{-1}): 629 (m), 594 (w), 450 (m).

Synthesis of $Cr[N(SiMe_3)_2]_2(tmeda)$ ***(2)***. $Cr[N(SiMe_3)_2]_2(thf)_2$ (87 mg, 0.17 mmol) was dissolved in *n*-hexane, and tmeda (28 mg, 0.24 mmol) was added. The color of the solution went from dark blue to light blue. After having stirred for 2.5 h at ambient temperature, the solvent was removed under vacuum, yielding an azur solid, which could be recrystallized from *n*-hexane. Yield: 68 mg, 83%. Anal. Calcd for $C_{18}H_{52}N_4Si_4Cr$: C 44.21, H 10.71, N 11.46. Found: C 43.27, H 10.61, N 11.17. DRIFT (KBr, cm^{-1}): 3025 (w), 3008 (w), 2957 (m), 2942 (m), 2896 (m), 2847 (w), 2807 (w), 1472 (m), 1440 (w), 1281 (w), 1247 (m), 1237 (s), 1187 (w), 1163 (w), 1116 (w), 1065 (w), 1016 (m), 1003 (w), 961 (s), 890 (m), 864 (s), 828 (s), 801 (m), 780 (m), 751 (m), 705 (w), 659 (m), 609 (w), 490 (w). IR (Nujol, cm^{-1}): 658 (m), 608 (w), 489 (vw), 390 (sh), 377 (m), 365 (sh), 226 (vw). UV−vis (*n*-hexane solution, λ_{max}, nm): 269 (sh), 630.

Synthesis of $\{Co[N(SiMe_3)_2]_2\}_2(\mu\text{-tmeda})$ ***(3)***. $Co[N(SiMe_3)_2]_2(thf)$ (125 mg, 0.27 mmol) was dissolved in *n*-hexane, and tmeda (64 mg, 0.55 mmol) was added. No color change was observed, and the reaction was stirred at ambient temperature for 3.5 h. Then the volatiles were removed under vacuum; crystallizing from *n*-hexane yielded turquoise green crystals. Yield: 111 mg, 92%. Anal. Calcd for $C_{18}H_{52}N_4Si_4Co$: C 41.15, H 10.13, N 9.60. Found: C 41.24, H 9.77, N 9.53. DRIFT (KBr, cm^{-1}): 3004 (w), 2947 (m), 2893 (w), 2846 (w), 2810 (w), 2800 (w), 1478 (w), 1462 (w), 1278 (sh), 1257 (s), 1244 (s), 1015 (w), 967 (s), 885 (m), 847 (s), 831 (s), 786 (m), 753 (m), 705 (w), 666 (m), 613 (w), 521 (w), 419 (w). IR (Nujol, cm^{-1}): 667 (w), 612 (vw), 521 (w), 365 (m). UV−vis (*n*-hexane solution, λ_{max}, nm): 330, 414, 600 (sh), 666.

Synthesis of $Cr[N(SiHMe_2)_2]_2(tmeda)$ ***(4)***. $Cr[N(SiMe_3)_2]_2(thf)_2$ (104 mg, 0.20 mmol) was dissolved in *n*-hexane, and tmeda (47 mg, 0.40 mmol) and $HN(SiHMe_2)_2$ (54 mg, 0.40 mmol) were added. The blue solution was stirred at ambient temperature for 3 h. Removing the solvent under vacuum yielded a purple solid, which gave purple crystals from toluene. Yield: 82 mg, 93%. Anal. Calcd for $C_{14}H_{44}N_4Si_4Cr$: C 38.85, H 10.25, N 12.94. Found: C 37.21, H 10.94, N 12.07 (unfortunately, we were not able to obtain better microanalysis data for this compound). DRIFT (KBr, cm^{-1}): 3013 (w), 2946 (m), 2894 (m), 2845 (w), 2807 (w), 2083 (m), 2047 (m), 2018 (m), 1468 (m), 1439 (w), 1356 (w), 1284 (m), 1240 (s), 1191 (w), 1164 (w), 1123 (w),1047 (s), 1025 (s), 948 (s), 920 (s), 891 (s), 789 (s), 756 (m), 704 (m), 672 (m), 628 (m), 485 (w). IR (Nujol, cm^{-1}): 660 (m), 609 (w), 380 (m). UV−vis (*n*-hexane solution, λ_{max}, nm): 282 (sh), 303, 793.

Synthesis of $Co[N(SiMe_3)_2][N(SiHMe_2)_2](tmeda)$ ***(5)***. $Co[N(SiMe_3)_2]_2(thf)$ (101 mg, 0.22 mmol) was dissolved in *n*-hexane, and tmeda (39 mg, 0.34 mmol) and $HN(SiHMe_2)_2$ (63 mg, 0.47 mmol) were added. The green solution turned dark green while stirring at ambient temperature for 3 h. Then the volatiles were removed under vacuum; crystallizing from *n*-hexane yielded dark green crystals. Yield: 67 mg, 64%. Anal. Calcd for $C_{16}H_{48}N_4Si_4Co$: C 41.08, H 10.34, N 11.98. Found: C 41.29, H 9.82, N 12.00. DRIFT (KBr, cm^{-1}): 3021 (w), 2952 (m), 2894 (m), 2850 (w), 2803 (w), 2121 (m), 2085 (m), 1466 (m), 1433 (w), 1282 (w), 1245 (s), 1044 (s), 1021 (m), 955 (s), 928 (s), 889 (vs), 836 (s), 787 (s), 757 (s), 704 (w), 674 (w), 629 (w), 421 (w).

Synthesis of $Co[N(SiHMe_2)_2]_2(tmeda)$ ***(6)***. $Co[N(SiMe_3)_2]_2(thf)$ (160 mg, 0.35 mmol) was dissolved in *n*-hexane, and tmeda (53 mg, 0.35 mmol) and $HN(SiHMe_2)_2$ (99 mg, 0.74 mmol) were added. The green solution was heated at 70 °C for 1 h in a pressure tube, turning dark brown toward the end. After cooling, the volatiles were removed under vacuum, and crystallizing from *n*-hexane yielded green crystals. Yield: 92 mg, 59%. Anal. Calcd for $C_{14}H_{44}N_4Si_4Co$: C 38.23, H 10.08, N 12.74. Found: C 38.26, H 9.76, N 12.52. DRIFT (KBr, cm^{-1}): 3011 (w), 2946 (m), 2893 (m), 2844 (w), 2799 (w), 2120 (m), 2078 (m), 1464 (m), 1443 (w), 1281 (w), 1241 (s), 1122 (w), 1043 (w), 1007 (m), 972 (s), 941 (s), 894 (s), 883 (s), 872 (s), 839 (s), 798 (s), 755 (m), 718 (m), 704 (m), 669 (m), 618 (m), 494 (w), 414 (w). IR (Nujol, cm^{-1}): 631 (w), 351 (w). UV−vis (*n*-hexane solution, λ_{max}, nm): 225 (sh), 316, 473, 632, 710.

Synthesis of $Mn[N(SiHMe_2)_2]_2(tmeda)$ ***(7)***. $Mn[N(SiHMe_2)_2]_2$ (86 mg, 0.27 mmol) was dissolved in *n*-hexane, and tmeda (63 mg, 0.54 mmol) was added. The colorless solution was stirred at ambient temperature for 1.5 h. Removing the solvent under vacuum yielded a white solid, which gave colorless crystals from *n*-hexane. Yield: 111 mg, 93%. Anal. Calcd for $C_{14}H_{44}N_4Si_4Mn$: C 38.58, H 10.18, N 12.86. Found: C 38.41, H 10.22, N 12.96. DRIFT (KBr, cm^{-1}): 3006 (w), 2949 (m), 2893 (m), 2847 (w), 2803 (w), 2049 (s), 1471 (m), 1446 (w), 1457 (m), 1434 (w), 1419 (w), 1409 (w), 1286 (w), 1239 (m), 1188 (w), 1163 (w), 1122 (w), 1033 (m), 1010 (m), 947 (s), 923 (s), 890 (s), 835 (s), 791 (s), 756 (s), 708 (m), 676 (m), 629 (m), 585 (w), 481 (w), 441 (w), 418 (w). IR (Nujol, cm^{-1}): 627 (m), 476 (w), 417 (w), 343 (m).

Synthesis of $Mn[N(SiMe_2Ph)_2]_2$ ***(8)***. $MnCl_2(thf)_{1.5}$ (100 mg, 0.43 mmol) was suspended in *n*-hexane, and $LiN(SiMe_2Ph)_2$ (264 mg, 0.85 mmol) in *n*-hexane was added. The mixture turned colorless. After stirring for 4 h at ambient temperature, no visible reaction had occurred and hence the reaction mixture was transferred into a pressure tube and heated to 70 °C for 6 h. LiCl was separated by

dx.doi.org/10.1021/ic5002682 | Inorg. Chem. 2014, 53, 4585−4597

centrifugation after cooling. The combined *n*-hexane fractions were dried under vacuum, yielding a yellowish solid. Crystallization from *n*-hexane gave colorless crystals. Yield: 205 mg, 76%. Anal. Calcd for $C_{32}H_{44}N_2Si_4Mn$: C 61.59, H 7.11, N 4.49. Found: C 61.76, H 6.96, N 4.57. DRIFT (KBr, cm^{-1}): 3128 (w), 3067 (w), 3051 (w), 3013 (w), 2995 (w), 2951 (m), 2894 (w), 1980 (w), 1961 (w), 1906 (w), 1891 (w), 1831 (w), 1776 (w), 1586 (w), 1563 (w), 1425 (m), 1406 (w), 1321 (w), 1305 (w), 1245 (s), 1190 (w), 1157 (w), 1109 (s), 1030 (w), 1002 (s), 923 (s), 933 (w), 842 (s), 791 (s), 772 (s), 732 (s), 705 (s), 675 (w), 642 (w), 476 (m), 463 (m). IR (Nujol, cm^{-1}): 646 (vw), 474 (m), 462 (m), 382 (m), 368 (sh), 299 (w).

*Synthesis of Cr[N(SiMe$_2$Ph)$_2$]$_2$ (**9**).* $CrCl_2$ (52 mg, 4.21 mmol) was suspended in thf and stirred for 40 min at ambient temperature. The solvent was evaporated off under vacuum, and the solid was suspended in *n*-hexane. Then $LiN(SiMe_2Ph)_2$ (245 mg, 8.42 mmol) in *n*-hexane was added, and the resulting green mixture was stirred at ambient temperature for 4 h. Afterward, LiCl was separated by centrifugation, and the combined *n*-hexane fractions were dried under vacuum. Recrystallization from pentane gave purple crystals first ($Cr[N(SiMe_2Ph)_2]_2(thf)_2$, 60 mg, 19%). Crystallization of the mother liquor yielded light green crystals. Yield: 158 mg, 60%. Anal. Calcd for $C_{32}H44N_2Si_4Cr$: C 61.89, H 7.14, N 4.51. Found: C 61.89, H 7.19, N 4.35. DRIFT (KBr, cm^{-1}): 3064 (w), 3045 (w), 2993 (w), 3010 (w), 2951 (m), 2895 (w), 1962 (vw), 1949 (vw), 1890 (vw), 1879 (vw), 1586 (w), 1485 (w), 1426 (m), 1403 (w), 1303 (w), 1246 (m), 1108 (m), 1091 (w), 1040 (m), 1028 (w), 998 (w), 987 (m), 912 (w), 830 (s), 811 (s), 801 (s), 773 (s), 733 (s), 701 (s), 679 (m), 638 (m), 489 (w), 473 (m), 448 (w). IR (Nujol, cm^{-1}): 646 (m), 473 (m), 390 (m). UV−vis (*n*-hexane solution, λ_{max}, nm): 261 (sh, $\pi \rightarrow \pi^*$ benzene ring), 323, 868.

*Synthesis of Co[N(SiMe$_2$Ph)$_2$]$_2$(thf) (**10**).* $CoCl_2(thf)_{1.25}$ (99 mg, 0.45 mml) was suspended in *n*-hexane, and $LiN(SiMe_2Ph)_2$ (262 mg, 0.90 mmol) in *n*-hexane was added. The mixture turned teal. After stirring for 6 h at ambient temperature, LiCl was separated by centrifugation. The combined *n*-hexane fractions were dried under vacuum, yielding a green solid. Crystallization from *n*-hexane gave green needles. Yield: 199 mg, 64%. Anal. Calcd for $CoN_2Si_4C_{32}H_{44}$: C 61.67, H 7.49, N 4.00. Found: C 61.68, H 6.54, N 4.09. DRIFT (KBr, cm^{-1}): 3131 (w), 3065 (w), 301 (w), 3017 (w), 2996 (w), 2952 (m), 2895 (w), 1980 (w), 1961 (w), 1906 (w), 1891 (w), 1831 (w), 1776 (w), 1586 (w), 1484 (w), 1425 (m), 1405 (w), 1321 (w), 1302 (w), 1246 (s), 1182 (w), 1109 (s), 1005 (s), 992(s), 931 (m), 835 (s), 800(s), 779 (s), 718 (s), 700 (s), 675 (m), 648 (m), 470 (m), 441 (w). IR (Nujol, cm^{-1}): 675 (w), 640 (w), 469 (m), 441 (m), 405 (m), 386 (m), 300 (w). UV−vis (*n*-hexane solution, λ_{max}, nm): 263 (sh, $\pi \rightarrow \pi^*$ benzene ring), 360, 520, 629, 791.

*Synthesis of Cr[N(SiMe$_2$Ph)$_2$]$_2$(thf)$_2$ (**11**).* $CrCl_2$ was suspended in thf, and $LiN(SiMe_2Ph)_2$ in thf was added, giving a teal suspension. After stirring for 3.5 h at ambient temperature, LiCl was separated by centrifugation. The thf was evaporated almost completely, and then pentane was added. Extraction with toluene and crystallization gave purple crystals. Yield: 255 mg, 47%. Anal. Calcd for $C_{40}H_{60}N_2O_2Si_4Cr$: C 62.78, H 7.90, N 3.66. Found: C 62.58, H 7.94, N 3.66. DRIFT (KBr, cm^{-1}): 3130 (w), 3066 (w), 3047 (w), 3016 (w), 2996 (w), 2953 (m), 2897 (w), 1948 (w), 1889 (w), 1819 (w), 1587 (w), 1486 (m), 1426 (m), 1405 (w), 1303 (w), 1248 (s), 1190 (w), 1109 (s), 1037 (m), 980 (m), 909 (s), 835 (s), 803 (s), 774 (s), 731 (s), 701 (s), 678 (s), 637 (m), 473 (m), 408 (m). IR (Nujol, cm^{-1}): 636 (w), 473 (m), 447 (w), 413 (m), 390 (sh), 366 (w), 347 (w), 288 (w), 246 (w). UV−vis (*n*-hexane solution, λ_{max}, nm): 262 (sh, $\pi \rightarrow \pi^*$ benzene ring), 325, 871.

Crystallographic Data Collection and Refinement. Crystals of **1** to **11** were grown by standard techniques from saturated solutions using *n*-hexane (**1**, **3**, **4**, **5**, **6**, **8**), toluene (**2**, **7**, **10**, **11**), or pentane (**9**) at −38 °C. Single crystals suitable for X-ray structure analyses were selected in a glovebox and coated with Paratone-N (Hampton Research). X-ray data for compounds **1** and **4** were collected on a Stoe IPDS II 2T diffractometer using Mo K_α radiation (λ = 0.71073 Å) and were corrected for Lorentz and polarization effects. Cell refinement and data reduction were performed by using X-Area.[67] The structure was solved by using SHELXS[68] and refined with SHELXL[68] against F^2. Numerical absorption correction has been done applying X-SHAPE/X-RED[69] based on an optimized crystal shape. Data collection for **2**, **5**, and **8** was performed on a Bruker SMART APEX II diffractometer using graphite-monochromated Mo K_α radiation (λ = 0.71073 Å). X-ray data for **3**, **6**, **7**, **9**, **10**, and **11** were collected on a Bruker APEX II DUO diffractometer equipped with a multilayer monochromator and Mo K_α radiation (λ = 0.71073 Å). Raw data were collected by using the program COSMO[70] and integrated and reduced with the program SAINT.[71] Corrections for adsorption effects were applied with SADABS.[72] The structures were solved by direct methods and refined with standard difference Fourier techniques (SHELXS/SHELXL).[68] All CIF files were checked at http://www.checkcif.iucr.org/. For further experimental details on refinement and crystallographic data see Tables 5−7. All plots were generated utilizing the programs Diamond 3.2i[73] and POV-Ray.[74] CCDC 976114 (**10**), 976115 (**11**), 976116 (**1**), 976117 (**2**), 976118 (**3**), 976119 (**4**), 976120 (**5**), 976121 (**6**), 976122 (**7**), 976123 (**8**), and 976123 (**9**) contain the supplementary crystallographic data for this paper. These data can be obtained free of charge from the Cambridge Crystallographic Data Centre via www.ccdc.cam.ac.uk/data_request/cif.

Table 6. Crystallographic Data for Bis(trimethylsilyl)amide Complexes 2 and 3

	2 (Cr)	**3** (Co)
fw (g/mol)	489.00	875.64
T (K)	100(2)	200(2)
space group	monoclinic $C2/c$	triclinic $P\bar{1}$
a, b, c (Å)	17.434(2), 8.597(1), 38.458(5)	9.1717(2), 14.4022(3), 21.3290(4)
α, β, γ (deg)	92.534(6)	71.411(1), 86.059(1), 84.980(1)
V (Å^3)	5758.2(13)	2657.69(9)
Z	8	2
d_{calc} (g/cm^3)	1.128	1.094
R_1[a]	0.0448	0.0341
wR_2[b]	0.1033	0.0913
GOF[c]	1.334	1.027

[a] $R_1 = \sum(|F_o| - |F_c|)/\sum|F_o|$, $F_o > 2\sigma(F_o)$. [b] $wR_2 = \{\sum[w(F_o^2 - F_c^2)^2]/\sum[w(F_o^2)^2]\}^{1/2}$. [c] $GOF = [\sum w(F_o^2 - F_c^2)^2/(n_0 - n_p)]^{1/2}$.

Table 7. Crystallographic Data of Bis(dimethylphenylsilyl)amide Complexes 8, 9, 10, and 11

	8 (Mn)	**9** (Cr)	**10** (Co)	**11** (Cr)
fw (g/mol)	623.99	621.05	700.09	765.26
T (K)	153(2)	100(2)	100(2)	100(2)
space group	monoclinic $P2_1/c$	monoclinic $P2_1/c$	monoclinic $P2_1/c$	monoclinic $P2_1/c$
a, b, c (Å)	22.819(2), 13.306(1), 23.498(2)	11.5550(4), 13.4514(5), 22.0416(7)	18.6495(4), 11.8450(2), 18.0184(4)	11.4798(6), 17.8748(8), 10.6447(5)
β (deg)	100.335(4)	99.178(1)	109.597(1)	111.877(2)
V (Å^3)	7019.1(9).	3382.1(2)	3749.8(1)	2027.0(2)
Z	8	4	4	2
d_{calc} (g/cm^3)	1.181	1.220	1.240	1.254
R_1[a]	0.0415	0.0264	0.0248	0.0273
wR_2[b]	0.1038	0.0720	0.0669	0.0832
GOF[c]	1.015	1.063	1.028	1.088

[a] $R_1 = \sum(|F_o| - |F_c|)/\sum|F_o|$, $F_o > 2\sigma(F_o)$. [b] $wR_2 = \{\sum[w(F_o^2 - F_c^2)^2]/\sum[w(F_o^2)^2]\}^{1/2}$. [c] $GOF = [\sum w(F_o^2 - F_c^2)^2/(n_0 - n_p)]^{1/2}$.

dx.doi.org/10.1021/ic5002682 | Inorg. Chem. 2014, 53, 4585−4597

■ ASSOCIATED CONTENT

Supporting Information

IR and UV−vis spectra as well as CIF files giving full crystallographic data for complexes **1**−**11**. This material is available free of charge via the Internet at http://pubs.acs.org.

■ AUTHOR INFORMATION

Corresponding Author

*E-mail: reiner.anwander@uni-tuebingen.de.

Notes

The authors declare no competing financial interest.

■ ACKNOWLEDGMENTS

Special thanks go to Daniel Werner at Monash University for solving the structure of $Co[N(SiHMe_2)_2]_2(tmeda)$ (**6**). Further thanks go to Dr. Klaus Eichele for technical assistance with the measurements of the magnetic moments and to Dr. Wolfgang Leis for help with UV−vis and FIR spectroscopy.

■ REFERENCES

(1) (a) Lappert, M. F.; Sanger, A. R.; Srivastava, R. C.; Power, P. P. *Metal and Metalloid Amides: Synthesis, Structure, and Physical and Chemical Properties*; Ellis Horwood Ltd: Chichester, 1980. (b) Lappert, M. F.; Protchenko, A.; Power, P. P.; Seeber, A. *Metal Amide Chemistry*; Wiley and Sons: Hoboken, NJ, 2009.

(2) Scandium: (a) Ghotra, J. S.; Hursthouse, M. B.; Welch, A. J. *J. Chem. Soc., Chem. Commun.* **1973**, 669. (b) Karl, M.; Harms, K.; Seybert, G.; Massa, W.; Fau, S.; Frenking, G.; Dehnicke, K. *Z. Anorg. Allg. Chem.* **1999**, *625*, 2055. Titanium: (c) Putzer, M. A.; Magull, J.; Goesmann, H.; Neumüller, B.; Dehnicke, K. *Chem. Ber.* **1996**, *129*, 1401. (d) Putzer, M. A.; Neumüller, B.; Dehnicke, K. *Z. Anorg. Allg. Chem.* **1998**, *624*, 1087. Vanadium: (e) Berno, P.; Minhas, R.; Hao, S.; Gambarotta, S. *Organometallics* **1994**, *13*, 1052. Chromium: (f) Köhn, R. D.; Kociok-Köhn, G.; Haufe, M. *Chem. Ber.* **1996**, *129*, 25. (g) Bradley, D. C.; Hursthouse, M. B.; Newing, C. W.; Welch, A. J. *J. Chem. Soc., Chem. Commun.* **1972**, 567. Iron: (h) Bradley, D. C.; Hursthouse, M. B.; Rodesiler, P. F. *J. Chem. Soc., Chem. Commun.* **1969**, 14. (i) Andersen, R. A.; Faegri, K.; Green, J. C.; Haaland, A.; Lappert, M. F.; Leung, W. P.; Rypdal, K. *Inorg. Chem.* **1988**, *27*, 1782. (j) Olmstead, M. M.; Power, P. P.; Shoner, S. C. *Inorg. Chem.* **1991**, *30*, 2547. Manganese and cobalt: (k) Bradley, D. C.; Hursthouse, M. B.; Malik, K. M. A.; Möseler, R. *Transition Met. Chem.* **1978**, *3*, 253. (l) Ellison, J. J.; Power, P. P.; Shoner, S. C. *J. Am. Chem. Soc.* **1989**, *111*, 8044. (m) Bradley, D. C.; Fisher, K. J. *J. Am. Chem. Soc.* **1971**, *93*, 2058. (n) Murray, B. D.; Power, P. P. *Inorg. Chem.* **1984**, *23*, 4584. Copper, silver, and gold: (o) James, A. M.; Laxman, R. K.; Fronczek, F. R.; Maverick, A. W. *Inorg. Chem.* **1998**, *37*, 3785. (p) Hitchcock, P. B.; Lappert, M. F.; Pierssens, L. J. M. *Chem. Commun.* **1996**, 1189. (q) Bunge, S. D.; Just, O.; Rees, J. W. S. *Angew. Chem., Int. Ed.* **2000**, *39*, 3082. Zinc, cadmium, and mercury: (r) Margraf, G.; Lerner, H. W.; Bolte, M.; Wagner, M. *Z. Anorg. Allg. Chem.* **2004**, *630*, 217. (s) Fisher, K. J.; Ayea, E. C. *Polyhedron* **1984**, *3*, 509. (t) Alyea, E. C.; Fisher, K. J.; Fjeldberg, T. *J. Mol. Struct.* **1985**, *127*, 325. (u) Alyea, E. C.; Fisher, K. J.; Fjeldberg, T. *J. Mol. Struct.* **1985**, *130*, 263.

(3) Fraser, R. R.; Mansour, T. S. *J. Org. Chem.* **1984**, *49*, 3442.

(4) (a) Malassa, A.; Agthe, C.; Görls, H.; Podewitz, M.; Yu, L.; Herrmann, C.; Reiher, M.; Westerhausen, M. *Eur. J. Inorg. Chem.* **2010**, *2010*, 1777. (b) Sulway, S. A.; Collison, D.; McDouall, J. J. W.; Tuna, F.; Layfield, R. A. *Inorg. Chem.* **2011**, *50*, 2521.

(5) (a) Yang, J.; Tilley, T. D. *Angew. Chem.* **2010**, *122*, 10384. (b) Yang, J.; Tilley, T. D. *Angew. Chem., Int. Ed.* **2010**, *49*, 10186.

(6) (a) Dey, M.; Gogoi, N. *Angew. Chem., Int. Ed.* **2013**, *52*, 12780. (b) Dey, M.; Gogoi, N. *Angew. Chem.* **2013**, *125*, 13014. (c) Lin, P.-H.; Smythe, N. C.; Gorelsky, S. I.; Maguire, S.; Henson, N. J.; Korobkov, I.; Scott, B. L.; Gordon, J. C.; Baker, R. T.; Murugesu, M. *J. Am. Chem. Soc.* **2011**, *133*, 15806. (d) Layfield, R. A.; McDouall, J. J. W.; Scheer, M.; Schwarzmaier, C.; Tuna, F. *Chem. Commun.* **2011**, *47*, 10623. (e) Zadrozny, J. M.; Atanasov, M.; Bryan, A. M.; Lin, C.-Y.; Rekken, B. D.; Power, P. P.; Neese, F.; Long, J. R. *Chem. Sci.* **2013**, *4*, 125.

(7) (a) Baxter, D. V.; Chisholm, M. H.; Gama, G. J.; Hector, A. L.; Parkin, I. P. *Chem. Vap. Deposition* **1995**, *1*, 49. (b) Suh, S.; Hoffman, D. M.; Atagi, L. M.; Smith, D. C. *Chem. Vap. Deposition* **2001**, *7*, 81. (c) Hubert-Pfalzgraf, L. G.; Touati, N.; Pasko, S. V.; Vaissermann, J.; Abrutis, A. *Polyhedron* **2005**, *24*, 3066. (d) Abrutis, A.; Hubert-Pfalzgraf, L. G.; Pasko, S.; Touati, N.; Kazlauskiene, V. *Vacuum* **2006**, *81*, 13. (e) Jiménez, E. d. L.; Javed, S.; Hoffman, D. M. *Inorg. Chim. Acta* **2009**, *362*, 385.

(8) Baxter, D. V.; Chisholm, M. H.; Gama, G. J.; DiStasi, V. F.; Hector, A. L.; Parkin, I. P. *Chem. Mater.* **1996**, *8*, 1222.

(9) (a) Cormary, B.; Dumestre, F.; Liakakos, N.; Soulantica, K.; Chaudret, B. *Dalton Trans.* **2013**, *42*, 12546. (b) Amiens, C.; Chaudret, B.; Ciuculescu-Pradines, D.; Colliere, V.; Fajerwerg, K.; Fau, P.; Kahn, M.; Maisonnat, A.; Soulantica, K.; Philippot, K. *New J. Chem.* **2013**, *37*, 3374.

(10) (a) Dumestre, F.; Chaudret, B.; Amiens, C.; Renaud, P.; Fejes, P. *Science* **2004**, *303*, 821. (b) Desvaux, C.; Amiens, C.; Fejes, P.; Renaud, P.; Respaud, M.; Lecante, P.; Snoeck, E.; Chaudret, B. *Nat. Mater.* **2005**, *4*, 750. (c) Lacroix, L.-M.; Lachaize, S. B.; Falqui, A.; Respaud, M.; Chaudret, B. *J. Am. Chem. Soc.* **2008**, *131*, 549. (d) Liakakos, N.; Cormary, B.; Li, X.; Lecante, P.; Respaud, M.; Maron, L.; Falqui, A.; Genovese, A.; Vendier, L.; Koïnis, S.; Chaudret, B.; Soulantica, K. *J. Am. Chem. Soc.* **2012**, *134*, 17922.

(11) Gerung, H.; Bunge, S. D.; Boyle, T. J.; Brinker, C. J.; Han, S. M. *Chem. Commun.* **2005**, 1914.

(12) For a key reference, see: Runte, O.; Priermeier, T.; Anwander, R. *Chem. Commun.* **1996**, 1385.

(13) Fischbach, A.; Anwander, R. *Adv. Polym. Sci.* **2006**, *204*, 155. (b) Zimmermann, M.; Anwander, R. *Chem. Rev.* **2010**, *110*, 6194.

(14) For examples, see: (a) Klimpel, M. G.; Anwander, R.; Tafipolsky, M.; Scherer, W. *Organometallics* **2001**, *20*, 3983. (b) Anwander, R.; Klimpel, M. G.; Martin Dietrich, H.; Shorokhov, D. J.; Scherer, W. *Chem. Commun.* **2003**, 1008. (c) Schrems, M. G.; Dietrich, H. M.; Törnroos, K. W. T.; Anwander, R. *Chem. Commun.* **2005**, 5922. (d) Sommerfeldt, H.-M.; Meermann, C.; Schrems, M. G.; Törnroos, K. W.; Frøystein, N. A.; Miller, R. J.; Scheidt, E. W.; Scherer, W.; Anwander, R. *Dalton Trans.* **2008**, 1899. (e) Litlabø, R.; Saliu, K.; Ferguson, M. J.; McDonald, R.; Takats, J.; Anwander, R. *Organometallics* **2009**, *28*, 6750. (f) Occhipinti, G.; Meermann, C.; Dietrich, H. M.; Litlabø, R.; Auras, F.; Törnroos, K. W.; Maichle-Mössmer, C.; Jensen, V. R.; Anwander, R. *J. Am. Chem. Soc.* **2011**, *133*, 6323. (g) Chen, J.; Luo, Y. *Organometallics* **2012**, *31*, 3730. (h) Hamidi, S.; Jende, L. N.; Dietrich, H. M.; Maichle-Mössmer, C.; Törnroos, K. W.; Deacon, G. B.; Junk, P. C.; Anwander, R. *Organometallics* **2013**, *32*, 1209. (i) Luo, R. Y.; Lei, Y.; Fan, S.; Wang, Y.; Chen, J. *Dalton Trans.* **2006**, *42*, 4040. (j) Jende, L. N.; Maichle-Mössmer, C.; Schädle, C.; Anwander, R. *J. Organomet. Chem.* **2013**, *744*, 74.

(15) Anwander, R. *Chem. Mater.* **2001**, *13*, 4419.

(16) Liang, Y.; Anwander, R. *Dalton Trans.* **2013**, *42*, 12521.

(17) (a) Horvath, B.; Horvath, E. *Ger. Offen.* DE 2653667, 1978. (b) Horvath, B.; Horvath, E. *Ger. Offen.* DE2653666 1978.

(18) Gauvin, R. M.; Buch, F.; Delevoye, L.; Harder, S. *Chem.—Eur. J.* **2009**, *15*, 4382.

(19) Roux, E. L.; Liang, Y.; Storz, M. P.; Anwander, R. *J. Am. Chem. Soc.* **2010**, *132*, 16368.

(20) Gerstberger, G.; Palm, C.; Anwander, R. *Chem.—Eur. J.* **1999**, *5*, 997.

(21) (a) Deschner, T.; Törnroos, K. W.; Anwander, R. *Inorg. Chem.* **2011**, *50*, 7217. (b) Deschner, T.; Klimpel, M.; Tafipolsky, M.; Scherer, W.; Törnroos, K. W.; Anwander, R. *Dalton Trans.* **2012**, *41*, 7319.

(22) Eppinger, J.; Spiegler, M.; Hieringer, W.; Herrmann, W. A.; Anwander, R. *J. Am. Chem. Soc.* **2000**, *122*, 3080.

(23) Nagl, I.; Scherer, W.; Tafipolsky, M.; Anwander, R. *Eur. J. Inorg. Chem.* **1999**, 1405.

(24) (a) Herrmann, W. A.; Anwander, R.; Munck, F. C.; Scherer, W.; Dufaud, V.; Huber, N. W.; Artus, G. R. J. *Z. Naturforsch. B* **1994**, *49*, 1789. (b) Anwander, R.; Runte, O.; Eppinger, J.; Gerstberger, G.; Herdtweck, E.; Spiegler, M. *J. Chem. Soc., Dalton Trans.* **1998**, 847. (c) Görlitzer, H. W. Ph.D. Thesis: *Amidische N-Donor-Komplexe der Seltenen Erden - Alternative Ligandensysteme für die Katalyse*; Anorganische-chemisches Institut der Technischen Universität München, 2000. (d) Dietrich, H. M.; Meermann, C.; Törnroos, K. W.; Anwander, R. *Organometallics* **2006**, *25*, 4316. (e) Schnitzlbaumer. PhD Thesis: M.D. *Seltenerdmetall-Alkoxide auf Periodisch Mesoporösem Silica*; Anorganisch-chemisches Institut der Technischen Universität München, 2006. (f) Rastätter, M.; Zulys, A.; Roesky, P. W. *Chem.—Eur. J.* **2007**, *13*, 3606. (g) Yuen, H. F.; Marks, T. J. *Organometallics* **2008**, *27*, 155. (h) Skår, H.; Seland, J. G.; Liang, Y.; Frøystein, N. Å.; Törnroos, K. W.; Anwander, R. *Eur. J. Inorg. Chem.* **2013**, 5969.

(25) Rabe, G. W.; Rhiengold, A. L.; Incarvito, C. D. *Z. Kristallogr.-New Cryst. Struct.* **2000**, *215*, 560.

(26) Crozier, A. R.; Bienfait, A. M.; Maichle-Mössmer, C.; Törnroos, K. W.; Anwander, R. *Chem. Commun.* **2013**, *49*, 87.

(27) (a) Sarazin, Y.; Roşca, D.; Poirier, V.; Roisnel, T.; Silvestru, A.; Maron, L.; Carpentier, J.-F. *Organometallics* **2010**, *29*, 569. (b) Michel, O.; Törnroos, K. W.; Maichle-Mössmer, C.; Anwander, R. *Chem.—Eur. J.* **2011**, *17*, 4964.

(28) (a) Hodgson, M. C.; Khan, M. A.; Wehmschulte, R. J. *J. Cluster Sci.* **2002**, *13*, 503. (b) Hill, J. B.; Talley, T. A.; Pennington, W. T.; Robinson, G. H. *J. Chem. Crystallogr.* **1994**, *24*, 61. (c) König, S. N.; Gerstberger, G.; Schädle, C.; Maichle-Mössmer, C.; Herdtweck, E.; Anwander, R. *Main Group Met. Chem.* **2013**, *36*, 169.

(29) Mansell, S. M.; Perandones, B. F.; Arnold, P. L. *J. Organomet. Chem.* **2010**, *695*, 2814.

(30) Liang, Y.; Anwander, R. *Dalton Trans.* **2006**, 1909.

(31) Mainz, V. V.; Andersen, R. A. *Inorg. Chem.* **1980**, *19*, 2165.

(32) Herrmann, W. A.; Huber, N. W.; Härter, P.; Denk, M.; Dyckhoff, F. *Chem. Ber.* **1992**, *125*, 117.

(33) Herrmann, W. A.; Huber, N. W.; Behm, J. *Chem. Ber.* **1992**, *125*, 1405.

(34) Deschner, T.; Lønstad, B.-T.; Widenmeyer, M.; Anwander, R. *J. Mater. Chem.* **2011**, *21*, 5620.

(35) Veith, M.; Koban, A.; Fries, K.; Spaniol, P.; Elsässer, R.; Rammo, A.; Huch, V.; Kleinsteuber, U. *Organometallics* **1998**, *17*, 2612.

(36) Chen, H.; Bartlett, R. A.; Dias, H. V. R.; Olmstead, M. M.; Power, P. P. *J. Am. Chem. Soc.* **1989**, *111*, 4338.

(37) Chen, H.; Olmstead, M. M.; Shoner, S. C.; Power, P. P. *J. Chem. Soc., Dalton Trans.* **1992**, 451.

(38) Alyea, E. C.; Fisher, K. J. *Polyhedron* **1986**, *5*, 695.

(39) Babcock, J. R.; Liable-Sands, L.; Rheingold, A. L.; Sita, L. R. *Organometallics* **1999**, *18*, 4437.

(40) Bürger, H.; Wannagat, U. *Monatsh. Chem.* **1964**, *95*, 1099.

(41) Shannon, R. D. *Acta Crystallogr., Sect. A* **1976**, *32*, 751.

(42) Bryan, A. M.; Long, G. J.; Grandjean, F.; Power, P. P. *Inorg. Chem.* **2013**, *52*, 12152.

(43) Glock, C.; Görls, H.; Westerhausen, M. *Inorg. Chim. Acta* **2011**, *374*, 429.

(44) Yang, S.; Du, Z.; Zhang, Y.; Shen, Q. *Chem. Commun.* **2012**, *48*, 9780.

(45) Lee, H. K.; Lam, C. H.; Li, S.-L.; Zhang, Z.-Y.; Mak, T. C. W. *Inorg. Chem.* **2001**, *40*, 4691.

(46) Kay Lee, H.; Suet Lam, T.; Lam, C.-K.; Li, H.-W.; Man Fung, S. *New J. Chem.* **2003**, *27*, 1310.

(47) Goebel, D. W.; Hencher, J. L.; Oliver, J. P. *Organometallics* **1983**, *2*, 746.

(48) Meermann, C.; Gerstberger, G.; Spiegler, M.; Törnroos, K. W.; Anwander, R. *Eur. J. Inorg. Chem.* **2008**, 2014.

(49) Margraf, G.; Schödel, F.; Sänger, I.; Bolte, M.; Wagner, M.; Lerner, H.-W. *Z. Naturforsch. B* **2012**, *67b*, 549.

(50) Panda, A.; Stender, M.; Olmstead, M. M.; Klavins, P.; Power, P. P. *Polyhedron* **2003**, *22*, 67.

(51) Bradley, D. C.; Hursthouse, M. B.; Ibrahim, A. A.; Abdul Malik, K. M.; Motevalli, M.; Möseler, R.; Powell, H.; Runnacles, J. D.; Sullivan, A. C. *Polyhedron* **1990**, *9*, 2959.

(52) Procopio, L. J.; Carroll, P. J.; Berry, D. H. *J. Am. Chem. Soc.* **1994**, *116*, 177.

(53) Boynton, J. N.; Merill, W. A.; Reiff, W. M.; Fettinger, J. C.; Power, P. P. *Inorg. Chem.* **2012**, *51*, 3212.

(54) Chen, H.; Bartlett, R. A.; Olmstead, M. M.; Power, P. P.; Shoner, S. C. *J. Am. Chem. Soc.* **1990**, *112*, 1048.

(55) Power, P. P. *Chem. Rev.* **2012**, *112*, 3482.

(56) Lin, C.-Y.; Guo, J.-D.; Fettinger, J. C.; Nagase, S.; Grandjean, F.; Long, G. J.; Chilton, N. F.; Power, P. P. *Inorg. Chem.* **2013**, *52*, 13584.

(57) Ni, C.; Rekken, B.; Fettinger, J. C.; Long, G. J.; Power, P. P. *Dalton Trans.* **2009**, 8349.

(58) Bryan, A. M.; Merill, W. A.; Reiff, W. M.; Fettinger, J. C.; Power, P. P. *Inorg. Chem.* **2012**, *51*, 3366.

(59) Cámpora, J.; Palma, P.; Pérez, C. M.; Rodríguez-Delgado, A.; Álvarez, E.; Guttiérrez-Puebla, E. *Organometallics* **2010**, *29*, 2960.

(60) Djukic, J.-P.; Dötz, K. H.; Pfeffer, M.; De Cian, A.; Fischer, J. *Organometallics* **1997**, *16*, 5171.

(61) Bradley, D. C.; Hursthouse, M. B.; Smallwood, R. J.; Welch, A. J. *J. Chem. Soc., Chem. Commun.* **1972**, 872.

(62) Evans, D. F. *J. Chem. Soc.* **1959**, 2003.

(63) Eppinger, J.; Herdtweck, E.; Anwander, R. *Polyhedron* **1998**, *17*, 1195.

(64) Brauer, G. *Handbuch der Päparativen Anorganischen Chemie*; Enke Verlag: Stuttgart, Germany, 1981.

(65) (a) Horvath, B.; Möseler, R.; Horvath, E. G. *Z. Anorg. Allg. Chem.* **1979**, *450*, 165. (b) Bradley, D. C.; Hursthouse, M. B.; Malik, K. M. A.; Möseler, R. *Transition Met. Chem.* **1987**, *3*, 253.

(66) (a) Kern, R. J. *J. Inorg. Nucl. Chem.* **1962**, *24*, 1105. (b) Byrne, E. K.; Theopold, K. H. *J. Am. Chem. Soc.* **1987**, *109*, 1282. (c) Zhao, H.; Clérac, R.; Sun, J. S.; Ouyang, X.; Clemente-Juan, J. M.; Gómez-Garcia, C. J.; Coronado, E.; Dunbar, K. R. *J. Solid State Chem.* **2001**, *159*, 281.

(67) Stoe & Cie. *X-Area 1.26*; Darmstadt, 2004.

(68) Sheldrick, G. M. *Acta Crystallogr., Sect. A: Found. Crystallogr.* **2008**, *64*, 112.

(69) (a) Stoe & Cie. *X-SHAPE 2.05, Crystal Optimization for Absorption Correction*; Darmstadt, 1996. (b) Stoe & Cie. *X-RED 1.26, Data Reduction for STAD4 and IPDS*; Darmstadt, 1996.

(70) Bruker ASX. *APEX v. 2008.5-0*; Madison, WI, 2008.

(71) Bruker AXS. *Bruker Saint v. 756A*; Madison, WI, 2009.

(72) Sheldrick, G. M. *SADABS v. 2008/1*; University of Göttingen: Göttingen, 2008.

(73) *Diamond-Crystal and Molecular Structure Visualization, Crystal Impact*; Dr. H. Putz & Dr. K. Brandenburg Gbr: Bonn, Germany, 2012.

(74) *POV-Ray v. 3.6*; Persistence of Vision Pty. Ltd.: Williamstown, Victoria, 2004.